MULTIAXIAL FATIGUE OF HIGH STRENGTH STEELS CONTAINING SMALL DEFECTS: MODELLING AND TESTS

Lucas Carneiro Araujo

Tese de Doutorado
Programa de Pós-Graduação em Ciências Mecânicas

FACULDADE DE TECNOLOGIA
UNIVERSIDADE DE BRASÍLIA

UNIVERSIDADE DE BRASÍLIA
FACULDADE DE TECNOLOGIA
DEPARTAMENTO DE ENGENHARIA MECÂNICA
PROGRAMA DE PÓSGRADUAÇÃO EM CIÊNCIAS MECÃNICAS

MULTIAXIAL FATIGUE OF HIGH STRENGTH STEELS CONTAINING SMALL DEFECTS: MODELLING AND TESTS

Lucas Carneiro Araujo

Orientador(a): José Alexander Araújo

TESE DE DOUTORADO

BRASÍLIA/DF: 23/07/2025

UNIVERSIDADE DE BRASÍLIA

FACULDADE DE TECNOLOGIA

DEPARTAMENTO DE ENGENHARIA MECÂNICA

PROGRAMA DE PÓSGRADUAÇÃO EM CIÊNCIAS MECÃNICAS

MULTIAXIAL FATIGUE OF HIGH STRENGTH STEELS CONTAINING SMALL DEFECTS: MODELLING AND TESTS

TESE SUBMETIDA AO PROGRAMA DE PÓS-GRADUAÇÃO EM CIÊNCIAS MECÂNICAS DA FACULDADE DE TECNOLOGIA DA UNIVERSIDADE DE BRASÍLIA, COMO PARTE DOS REQUISITOS NECESSÁRIOS PARA OBTENÇÃO DO GRAU DE DOUTOR EM CIÊNCIAS MECÂNICAS.

APROVADA POR:

Prof. José Alexander Araújo, D. Phil. (UnB)

(Orientador)

Prof. Lucival Malcher, Dr. (UnB/Inegi-Feup)

(Examinador Interno)

Prof. Rui Ricardo Loureiro Amaral, Dr. (Inegi-Feup)

(Examinador Externo)

Prof. Marcos Venícius Soares Pereira, PhD. (Puc-Rio)

(Examinador Externo)

BRASÍLIA/DF, 23 de julho de 2025.

FICHA CATALOGRÁFICA

CARNEIRO ARAUJO, LUCAS

Multiaxial Fatigue of High Strength Steels Containing Small Defects: Modelling and Tests [Distrito Federal] 2025.

xvi, 86p.210x297mm (PPGCM/FT/Unb, Doutor, Ciências Mecânicas, 2025).

Tese de Doutorado – Universidade de Brasília. Faculdade de Tecnologia.

Programa de Pós-Graduação em Ciências Mecânicas.

1. MULTIAXIAL FATIGUE 2. SMALL DEFECTS

3. NEW MODEL 4. PRINCIPAL STRESSES AMPLITUDE

I.ENM/FT/UnbII.Brasília

REFERÊNCIA BIBLIOGRÁFICA

ARAUJO, L.C., Multiaxial Fatigue of High Strength Steels Containing Small Defects: Modelling and Tests. Tese de Doutorado em Ciências Mecânicas. Programa de Pós-Graduação em Ciências Mecânicas, Universidade de Brasília – Faculdade de Tecnologia, Brasília, DF, 86p, 2025.

CESSÃO DE DIREITOS

AUTOR: Lucas Carneiro Araujo

TÍTULO: Multiaxial Fatigue of High Strength Steels Containing Small Defects: Modelling and Tests

GRAU: Doutor ANO: 2025

_____

LUCAS CAREIRO ARAUJO

AGRADECIMENTOS

Agradeço primeiramente a Deus por me permitir trilhar nesse caminho e por prepará-lo, como sempre, da melhor forma, colocando nele as pessoas certas para me auxiliar, me favorecendo de oportunidades e não deixando nenhum mal me afligir.

Agradeço a minha família por todo o apoio e amor transmitidos. Agradeço em especial aos meus pais Paulo e Valdirene por sempre me incentivarem e por não medirem esforços para que eu pudesse seguir nos estudos. Agradeço também aos meus irmãos Sergio e Matheus e aos meus primos, pelos momentos de descontração e alegria durante esses anos.

Agradeço a minha esposa, Sayra, por estar sempre ao meu lado, mesmo que a distância em alguns momentos, pela paciência e por todos os anos de companheirismo e amor. Agradeço também a sua família por me acolher de braços abertos.

Agradeço ao meu orientador José Alexander, sem o qual o início dessa jornada teria sido muito mais difícil, por todo o conhecimento transmitido, pelos bons conselhos de vida, pelos momentos gastos para me auxiliar e por sempre estar em busca de condições melhores para o desenvolvimento das pesquisas no laboratório.

Agradeço a todos os amigos que conquistei durante esses anos no laboratório, os "Fadigados", pelo apoio e companheirismo, essa jornada teria sido muito mais difícil sem vocês.

Agradeço a todos os técnicos, em especial ao Wesley pela grande dedicação e compromisso, aos professores do programa que me auxiliaram de alguma forma, esclarecendo minhas dúvidas, ensinando a operar os equipamentos e mantendo o laboratório em condições de funcionamento.

Dedico este trabalho aos meus pais, que sempre suportaram todas as cargas cíclicas da vida sem nunca atingirem o limite de resistência, e à minha esposa cujo amor foi o alívio de tensões que impediu que as trincas se propagassem.

RESUMO

FADIGA MULTIAXIAL DE AÇÕS DE ALTA RESISÊNCIA CONTENDO PEQUENOS DEFEITOS: MODELAGEM E TESTES

Autor(a): Lucas Carneiro Araujo
Orientador(a): José Alexander Araújo
Programa de Pós-Graduação em Ciências Mecânicas
Brasília, 2025.

Pequenos defeitos e condições de tensão multiaxial são comuns em componentes reais de engenharia, mas o impacto combinado desses elementos sobre a resistência à fadiga ainda foi pouco investigado na literatura. Este estudo em sua primeira parte tem como objetivo investigar o comportamento de fadiga de alto ciclo do aço AISI 4140, considerando tanto as inclusões não metálicas inerentes quanto microfuros superficiais introduzidos artificialmente. Foram realizados testes de fadiga axial/torcional sob carregamento em fase e fora de fase, com proporções variáveis de amplitudes de tensão normal e de cisalhamento. A análise microscópica dos espécimes que falharam revelou que a formação de trincas é dominada predominantemente pelas tensões de tração na maioria das condições de carregamento. Previsões de resistência à fadiga foram feitas com base em um critério de plano crítico que usa o parâmetro √área, demonstrando precisão suficiente para aplicações de engenharia e correlacionando com sucesso a direção das trincas.

Além disso, nas partes seguintes desse estudo, é apresentado e avaliado um novo modelo de fadiga multiaxial para materiais metálicos que contêm pequenos defeitos. Este modelo correlaciona o limite de fadiga uniaxial obtido a partir do parâmetro √área, de um aço de alta resistência contendo pequeno defeito, com valores associados à amplitude das tensões principais, cujo cálculo para carregamentos não proporcionais não é trivial. O desempenho do modelo foi validado com dados experimentais dos aços AISI 4140 e 4340 sob várias condições de carregamento, incluindo espécimes apenas com seus defeitos naturais e espécimes com microfuro superficial. O modelo proposto forneceu estimativas de resistência à fadiga satisfatórias, com uma calibração simples, rápida e econômica o que é de grande interesse para fins de cálculos de engenharia.

ABSTRACT

MULTIAXIAL FATIGUE OF HIGH STRENGTH STEELS CONTAINING SMALL DEFECTS: MODELLING AND TESTS

Author: Araujo, Lucas Carneiro
Advisor: Araújo, José Alexander
PhD in Mechanical Sciences
Brasília, 2025.

Small defects and multiaxial stress conditions are common in real-world engineering components, yet the combined impact of these factors on fatigue strength has been underexplored in the literature. The first part of this study aims to investigate the high-cycle fatigue behavior of AISI 4140 steel, considering both inherent non-metallic inclusions and artificially introduced surface microholes. Axial/torsional fatigue tests were performed under in-phase and out-of-phase loading, with varying ratios of normal and shear stress amplitudes. Microscopic analysis of the failed specimens revealed that crack formation was predominantly driven by tensile stresses under most loading conditions. Fatigue strength predictions were made using a critical plane criterion based on the √area parameter, demonstrating sufficient accuracy for engineering applications and successfully correlating the crack direction.

Furthermore, a new multiaxial fatigue model for metallic materials containing small defects is introduced and evaluated in the following parts of the study. This model correlates the uniaxial fatigue limit derived from the √area parameter of high-strength steel containing small defects with values associated with the amplitude of the principal stresses, whose calculation under non-proportional loading is non-trivial. The model's performance was validated with experimental data from AISI 4140 and 4340 steels under various loading conditions, including specimens with only their natural defects and specimens with a superficial microhole. The proposed model provided satisfactory fatigue strength estimates, with a simple, fast, and cost-effective calibration process, which is of great interest for engineering calculation purposes.

SUMMARY

TABLES

FIGURES

1. INTRODUCTION

1.1 Motivation

Fatigue is one of the primary failure mechanisms in mechanical components subjected to cyclic loading, even at stress levels below the material's yield strength. This phenomenon is particularly critical in materials with small defects, such as micro flows, non-metallic inclusions, pores, and material inhomogeneities that are well-recognized as factors that increase fatigue failure in mechanical components [1–5]. As mentioned in ref. [6], these imperfections are inherent to the manufacturing processes, and their complete elimination would require extremely high levels of quality control, which is not economically viable [7]. Consequently, predicting the effect of such defects on the fatigue strength of metallic materials has become increasingly necessary, fostering extensive research over the past decades.

The impact of small defects and non-metallic inclusions on fatigue strength has been widely studied over the years [2,8]. The presence of these imperfections intensifies stress concentration, accelerating fatigue crack initiation and reducing the component's working life [9,10]. The fatigue strength of high-strength steels is considerably affected by the presence of microscopic defects. This effect has been evidenced in real-world failures, such as the recent cases of crankshaft fractures in Brazilian thermoelectric power plants (Fig. 01). After investigation, it was determined that the cause of these failures was the presence of numerous non-metallic inclusions in the material. These crankshafts, made of DIN 42CrMo4 steel (hereinafter referred to as AISI 4140 steel due to its chemical similarity) and DIN 34CrNiMo6 steel (hereinafter referred to as AISI 4340 steel due to its chemical similarity), suffered premature fatigue damage due to these impurities. This type of failure can cause major disruption in the industry and extremely high financial losses.

Crankshafts are subjected to cyclic loading conditions due to radial forces generated by combustion pressure, transmitted by pistons and connecting rods. This leads to harmonic torsion combined with cyclic bending, creating conditions for fatigue damage over time. Ideally, these components are designed for infinite life, enduring millions of loading cycles. However, inadequate consideration or complete disregard of small defects in the design process can lead to incorrect material specifications and fatigue failures, as cracks tend to initiate in these regions, as in the case mentioned above [11]

a

b

Figure 1. (a) crankshaft of a thermoelectric generator that failed in a Brazilian power plant, (b) fatigue crack in the crankshaft.

In fact, numerous studies report fatigue failures caused by small defects and non-metallic inclusions in critical engineering components, including wind turbine gearboxes, railway wheels, pipelines, turbine blades, and crankshafts [12–15]. Many of these components are subjected to time-varying multiaxial stresses throughout their operational life. Despite extensive research on fatigue in materials with small defects, most studies have been conducted under uniaxial loading conditions. Investigations into multiaxial fatigue behavior in the presence of small defects remain scarce, though interest in this area has grown significantly in recent years. Given the prevalence of real-world failures and the complex stress states experienced by critical components, the study of multiaxial fatigue in defective materials is an increasingly relevant and urgent topic.

1.2 State of the art

One widely employed parameter for estimating the fatigue strength of metals with small defects is the √area parameter, which represents the square root of the

projected defect area perpendicular to the load direction [16]. This method has proven effective in predicting the uniaxial fatigue limit across both conventional and additively manufactured metals, particularly in high and very high-cycle fatigue regimes [2].

In the past two decades, significant efforts have been made to develop predictive models for fatigue strength in metals with small defects subjected to multiaxial stress conditions. This research holds great relevance for fatigue design in industrial applications, where engineering components typically endure multiaxial stresses from notches and combined loading. One of the earliest attempts to create a multiaxial fatigue limit criterion for small defects was proposed by Endo in 1999 [17], where a fatigue parameter was defined by a combination of the maximum and minimum principal stress amplitudes, and this was compared to the uniaxial fatigue limit obtained from the √area approach [16]. Subsequent research by Endo and colleagues expanded this formulation to account for phase difference and mean stress effects on the fatigue limit of defects under combined axial and shear loading [8,18–20]. Another approach, proposed by Nadot [21–23], addresses the small defect fatigue problem by incorporating the type, morphology, position, size, and loading conditions into the fatigue strength prediction. This method involves two key steps: (i) stress analysis of the defect using an elastic-plastic material model, followed by (ii) application of a classical multiaxial fatigue criterion modified by parameters based on the defect's stress gradient and size [6]. Recent years have also seen a growing interest in studying defects intrinsic to additive manufacturing, such as porosities, shrinkage, and lack of fusion, prompting the development of non-destructive characterization techniques integrated with fatigue life prediction models [24–27].

As presented in [6], in related works, Araujo and co-workers [11,28,29] have demonstrated that classical multiaxial fatigue criteria, such as the Findley criterion and the modified Wöhler curve method, can be adapted to account for small defects in fatigue limit predictions. This is achieved by calibrating these criteria with the uniaxial and torsional fatigue limits obtained from the √area approach. Other studies [30,31] have shown that this methodology can also be successfully applied to the Carpinteri criterion. More recently, Araujo [32] proposed a parameter similar to the Smith–Watson–Topper parameter, but based on the amplitude and maximum values of the principal stress instead of the normal stress. Additionally, Castro et al. [33,34] refined the application of the critical plane approach for small defects by introducing a directionally dependent fatigue strength criterion to address situations where the projected area varies with the plane, as

observed in irregularly shaped defects. This concept was implemented using the Walker parameter, yielding good agreement between predictions and experimental data.

1.3 Objective

The objective of this study is to develop and evaluate methodologies for fatigue design in materials that are either internally flawed or contain small surface defects, particularly when subjected to multiaxial loading. It addresses combined axial and torsional loading under both proportional and non-proportional conditions. The study will assess a critical plane model, proposed by Castro et al. [33,34] to account for the influence of small defects in multiaxial fatigue, as well as this study will evaluate a new multiaxial fatigue model developed by the author and co-workers [35,36].

For incorporating the effects of inclusions and defects into multiaxial models, it is proposed to calibrate the models using fatigue limits associated with the √area parameter. This parameter, which reflects the projected area of a defect perpendicular to the loading direction, is determined by using extreme value statistics for internal inclusions and is calculated for known-sized surface defects. The √area approach has been shown to effectively predict fatigue limits in high-cycle fatigue regimes for both conventional and additively manufactured metals [1,2,16,37].

The validity of these adapted critical plane models will be tested by comparing their predictions to experimental data obtained from specimens manufactured from both AISI 4140 and AISI 4340 steels. These materials are widely used in the production of crankshafts for stationary generator sets and are known to contain non-metallic inclusions that can act as stress concentrators, promoting fatigue crack initiation. The specimens were tested under two conditions: smooth, containing only their natural defects, and with artificially introduced surface microholes. This approach allows for a comprehensive evaluation of how both natural microstructural inhomogeneities and controlled surface defects influence fatigue behavior under multiaxial loading.

By analyzing the performance of the models across these varied conditions, the study aims to improve the reliability of fatigue strength estimations for components exposed to complex loading in real-world applications. This dual-material, dual-condition testing framework ensures that the proposed methodologies are robust and can be adapted for different types of steel used in critical mechanical components.

1.4 Organization of the thesis

This work is structured as follows:

- The first chapter of this work presents the motivational aspects that lead to this study, followed by a brief review of the state of the art, presenting studies already developed related to the topic, then presents the objectives that are expected to be achieved with the studies developed, as well as this section that explains how the work is organized.
- The subsequent chapters (2, 3, 4, and 5) are formatted as independent scientific articles, each providing a brief review of relevant concepts, outlining the methodology employed, presenting and analyzing the results, and drawing conclusions.
- Chapter 6 presents the general conclusions of the work, obtained from all the analyses carried out and based on the initial objectives presented.
- Some suggestions for future work are presented in the following section.
- At the end of the work, all the references are included.

Chapters 2, 3, and 4 consist of a reproduction of articles previously published by the author during the doctoral research. Chapter 5 presents a new article with new data, offering an extended evaluation of the developed model, which is in process of submission to a scientific journal.

1.5 Publications

The following publications constitute the work carried out in this thesis:

In International Journals:

- **Araujo LC**, da Costa RA, Araújo JA, de Castro FC. Effect of natural and artificial defects on multiaxial fatigue of 4140 steel. International Journal of Fatigue (96% percentile in Scopus) 2024
- **Araujo LC**, Malcher L, de Oliveira D, Araújo JA. A new multiaxial fatigue endurance model for high strength steels taking into account the presence of small defects International Journal of Fatigue (96% percentile in Scopus) 2024

In International Conferences:

- **Araujo LC**, Ferreira JL de A, Ziberov M, Araújo JA. Assessing Fatigue in Materials with Small Defects: A New Multiaxial Model Based on Principal Stress Amplitudes. Procedia Structural Integrity 2024 - Fatigue Design 2023
- **Araujo LC**, Oliveira D de, Araújo JA. A New Multiaxial Fatigue Model for High Strength Steels Taking into Account the Presence of Small Defects. Proceedings of the 13th International Conference on Multiaxial Fatigue and Fracture (ICMFF13), 2022.

2. EFFECT OF NATURAL AND ARTIFICIAL DEFECTS ON MULTIAXIAL FATIGUE OF 4140 STEEL

This chapter is a reproduction of the following publication.

- Araujo LC, da Costa RA, Araújo JA, de Castro FC. Effect of natural and artificial defects on multiaxial fatigue of 4140 steel. International Journal of Fatigue 2024;178

Abstract

Despite the prevalence of small defects and multiaxial stress conditions in load-bearing engineering components, their combined effect on fatigue strength is not usually considered in the literature. In this study, the high-cycle fatigue behavior of 4140 steel with its inherent non-metallic inclusions, and with an artificial surface microhole is investigated under axial/torsional loading. The multiaxial fatigue tests were performed under in-phase and out-of-phase loading, employing different ratios between the shear and axial stress amplitudes. Microscopy of failed specimens indicated a tensile-dominated crack formation mechanism in most of the tests. Analysis of the test data using a $\sqrt{area}$-based critical plane criterion showed that predictions of fatigue strength and crack direction can be made with sufficient accuracy for engineering calculations.

Keywords: 4140 steel; defects; fatigue strength; multiaxial fatigue; critical plane

2.1 Introduction

Small flaws, non-metallic inclusions, and inhomogeneities in mechanical components are known to aggravate the fatigue process [1–5]. They are inherent to the manufacturing process and eliminating them would require very high-quality control during manufacturing, which is economically unfeasible [7]. Therefore, the prediction of the influence of defects on the fatigue strength of metallic materials has become necessary and has been an active research field over the past decades. A parameter that is widely used to predict the fatigue strength of metals with small defects is the $\sqrt{area}$, the square

root of the projected area of a defect perpendicular to the loading direction [16]. This approach has proven successful in estimating the uniaxial fatigue limit of conventional and additively manufactured metals in high and very high-cycle fatigue regimes [2].

From an engineering perspective, the combined action of small defects and multiaxial loading should be properly taken into account to avoid undesirable fatigue failures. For example, case studies [12–15] can be found where critical components (e.g., gearboxes in wind turbines, railway wheels, pipelines, turbine blades, and crankshafts) failed from small defects subjected to time-varying multiaxial stresses. Moreover, in a recent episode in Brazil, fatigue failures occurred in crankshafts of thermoelectric generators. These crankshafts were made of AISI 4140 (DIN 42CrMo4) or AISI 4340 (DIN 34CrNiMo6) steel, which contained non-metallic inclusions formed during steelmaking.

Over the last two decades, efforts have been made to develop predictive models for the fatigue strength of metals with small defects under multiaxial stress histories. This research is important to fatigue design in an industrial context since engineering components generally experience multiaxial stresses caused by notches and multiple loads. One of the first attempts to formulate a multiaxial fatigue limit criterion for small defects can be traced back to the 1999 paper by Endo [17]. In this criterion, a fatigue parameter defined by a combination of the maximum and minimum principal stress amplitudes is compared to the uniaxial fatigue limit derived from the $\sqrt{area}$ approach [16]. Subsequent research by Endo and co-workers extended the original formulation to include the effects of phase difference and mean stress on the fatigue limit of a defect under combined axial and shear stresses [8,18–20]. Another view on the small defect fatigue problem has been proposed by Nadot [21–23]. To incorporate the effects of the type, morphology, position, size, and loading on the fatigue strength of defects, this author has considered an approach based on two steps: (i) a stress analysis of the defect using an elastic-plastic material model; and (ii) the application of a classical multiaxial fatigue criterion modified by parameters that depend on the stress gradient at the hot spot of the defect and on the size of the defect. In recent years, intrinsic additive manufacturing defects such as porosities, shrinkage, and lack of fusion have been investigated. This research led to the development of non-destructive characterization techniques coupled with models for predicting fatigue life and strength [24–27].

Araujo and co-workers [11,28,29] have recently suggested that classical multiaxial fatigue criteria (such as the Findley criterion and the modified Wöhler curve

method) can be readily adapted to incorporate the effect of small defects on the fatigue limit of metals. This was accomplished by calibrating a given criterion with the uniaxial and torsional fatigue limits derived from the $\sqrt{area}$ approach. Studies [30,31,38] have shown that this procedure can also be successfully applied to the Carpinteri criterion. More recently, Araujo [32] developed a parameter similar to the Smith–Watson–Topper but using the amplitude and maximum values of the principal stress, instead of the normal stress. Castro et al. [33,34] proposed a refinement of the application of the critical plane approach to small defects. A directionally dependent fatigue strength was introduced into the critical plane search to deal with situations where the projected area varies with the plane, as occurs for defects with irregular shapes. The idea was implemented using the Walker parameter and good agreement between predictions and test data was achieved.

In this study, new fatigue test data as well as experimental results reported earlier [11,28,29] were used to investigate the fatigue strength of AISI 4140 steel at 2×10^6 cycles. The tests were performed under fully reversed conditions and included axial, torsional, and axial-torsional (in-phase and out-of-phase) loading histories. The material was assessed considering two conditions: (i) only with its natural defects, that is, the non-metallic inclusions; and (ii) with a cylindrical blind microhole artificially introduced into the surface of the specimens. The dimensions of the microhole were 550 μm in depth and diameter, to simulate possible surface defects much larger than the inclusions observed in the material. A critical plane multiaxial criterion for small defects [33,34] was evaluated using the fatigue test data. Comparisons between measured and predicted critical plane directions and fatigue strengths were performed. The analysis was made considering two procedures for determining the constants of the criterion, one based on fatigue strengths calculated from $\sqrt{area}$ -based formulas and another using experimentally measured fatigue strengths.

2.2 Experimental Program

2.2.1 Material and specimens

The material investigated in this study was AISI 4140 (42CrMo4) steel, which was oil quenched and tempered in the 530 - 630 °C range. The material was removed from crankshafts of stationary generators that failed due to fatigue during operation. Table

1 lists the chemical composition of the material, which was obtained by optical emission analysis according to ASTM standard A751.

The microstructure of the 4140 steel is shown in Fig. 2, where the transverse and longitudinal sections were defined relative to the longitudinal axis of the specimen (refer to Fig. 3). The metallographic samples were polished and etched with 5% nitric acid solution in ethanol and examined using optical microscopy. It is possible to identify in the microstructure regions with thick phases of light tone that correspond to α-ferrite phase; it can also be observed elongated regions with α-ferrite and cementite (Fe3C) phases, which are characteristic of tempered martensite. The non-metallic inclusions were analyzed by Energy Dispersive X-ray Spectroscopy, which revealed that their chemical composition was mainly composed of aluminum (Al), silicon (Si), and oxygen (O).

Table 1. Chemical composition of SAE 4140 (wt. %).

C	Si	Mn	P	S	Cr	Mo	Fe
0.41	0.08	0.82	0.004	0.006	1.01	0.25	Balance

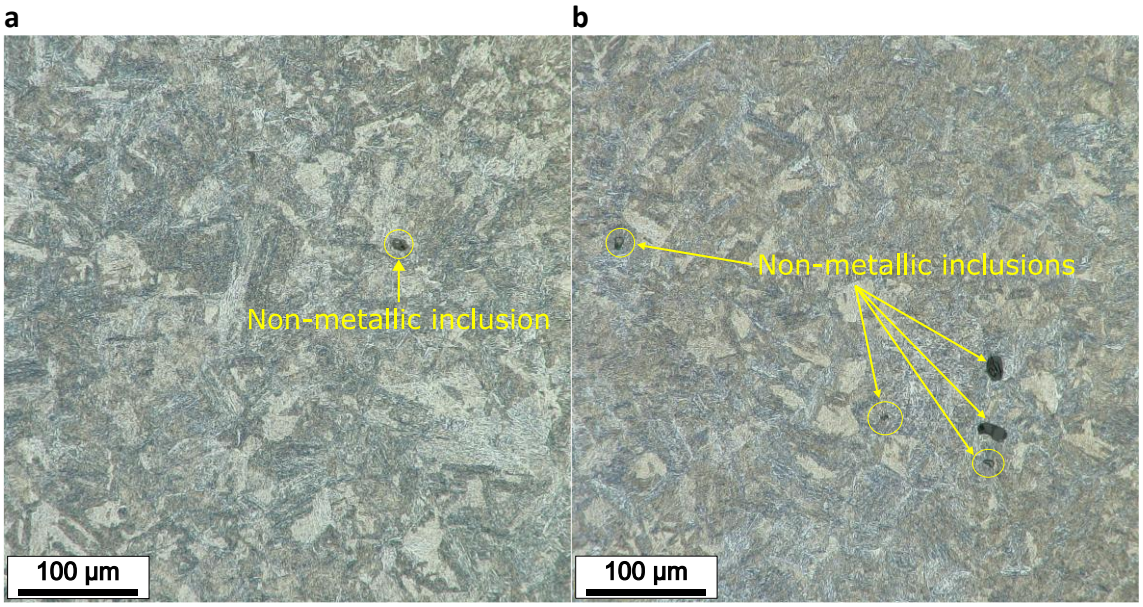

Figure 2. Microstructure of 4140 steel: (a) transverse section and (b) longitudinal section of the solid cylindrical specimen shown in Fig. 3.

The average areas of the α-ferrite phase were measured using a confocal microscope, and for the transverse section, the average area was 277 µm². The

corresponding measures for the longitudinal section were 256 μm². These measures indicated that there were no significant differences in the microstructure in different section planes of the material.

Table 2 lists the mechanical properties of the 4140 steel measured by the authors in a standard tensile test. The Vickers hardness was measured using an applied load of 100 kgf. Note that the tensile properties given here are slightly different from those reported in Refs. [11,28,29] because the previous values were the ones provided by the manufacturer.

Table 2. Mechanical properties of AISI 4140 steel.

Young's modulus (GPa)	0.2%-offset yield stress (MPa)	Ultimate tensile strength (MPa)	Elongation (%)	Vickers hardness (kgf/mm^2)
202	647	932	20	320

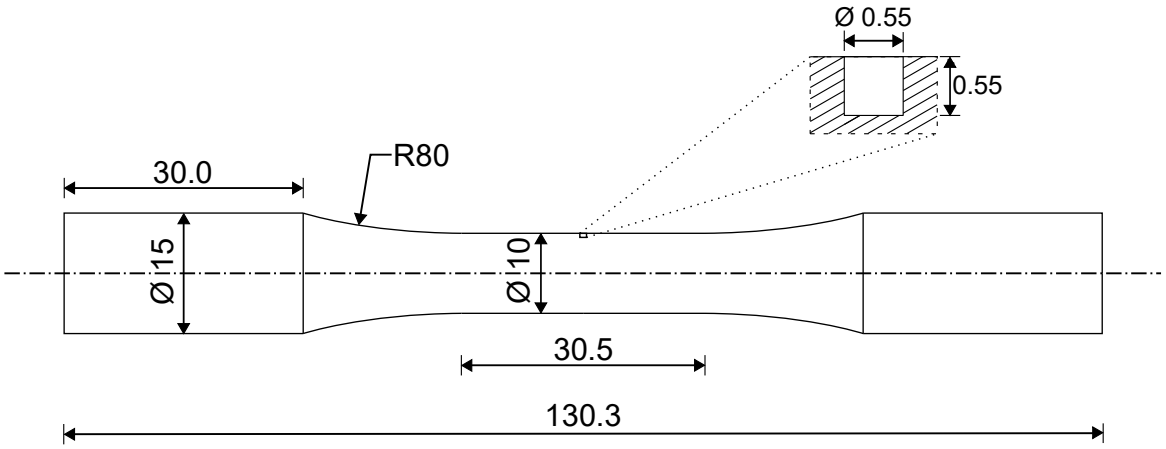

Figure 3. Specimen used in the fatigue tests and detail in the case of specimens with cylindrical blind microhole (dimensions in mm).

The geometry of the solid cylindrical specimens used in the fatigue tests is shown in Fig. 3. The specimens were machined from material cut from a crankshaft and polished with sandpaper to impart a maximum surface roughness of 0.2 μm. Two types of specimens were investigated: (i) plain specimens without any visible surface defect; and (ii) specimens with a cylindrical blind microhole with a diameter and depth of 550 μm, which were artificially introduced into the specimen surface using a CNC XH7132

milling machine. The purpose of these microholes was to simulate surface defects much larger than the inclusions of the material, which may originate in a component by external action (e.g., handling operation). The machining process was carried out in such a way as to minimize residual stresses, and no further treatments were carried out to relieve these stresses.

2.2.2 Fatigue tests

The fatigue tests were performed under load control. An MTS 809 servo-hydraulic test system, with a capacity of 100 kN in axial force and 1100 N·m in torque, was employed for the axial/torsional tests. Uniaxial fatigue tests were also conducted in an MTS 810 servo-hydraulic test system with a force capacity of 100 kN. The stresses acting on a material volume element of the specimen surface were defined based on the coordinate system shown in Fig. 4. Moreover, the stress histories used in the fatigue tests were as follows:

$$\sigma_x = \sigma_{xa} \sin \omega t \tag{1}$$

$$\tau_{xy} = \tau_{xya} \sin(\omega t + \delta) \tag{2}$$

where σ_x is the axial stress, τ_{xy} is the shear stress, the subscript a denotes amplitude, ω is the angular frequency, δ is the phase difference between the axial and shear stresses, and t denotes time. Fig. 4 also shows the stress components relative to a coordinate system rotated by an angle θ about the z-axis. They will be used in Section 2.3 in the formulation of a critical plane fatigue criterion for small defects.

The stress paths used in the fatigue tests are shown in Fig. 5. The tests were performed under fully reversed loading and were characterized by the ratio $\lambda = \tau_{xya}/\sigma_{xa}$ between the shear and axial stress amplitudes. The tension-compression and torsion tests have $\lambda = 0$ and ∞, respectively. The in-phase and 90º out-of-phase tests were conducted with values of $\lambda = 0.5$, 1, and 2.

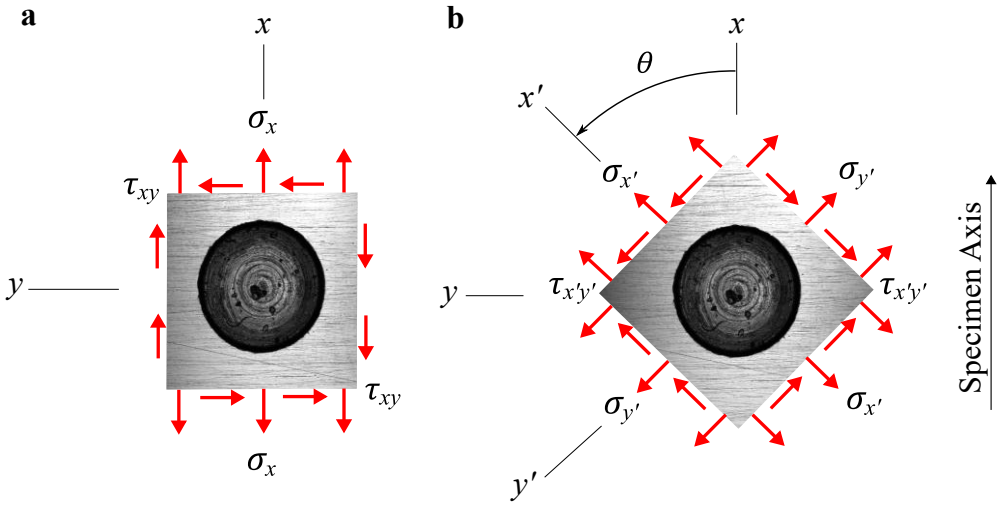

Figure 4. (a) Material volume element with microhole under axial and shear stresses. (b) Stresses acting on the microhole relative to a rotated coordinate system.

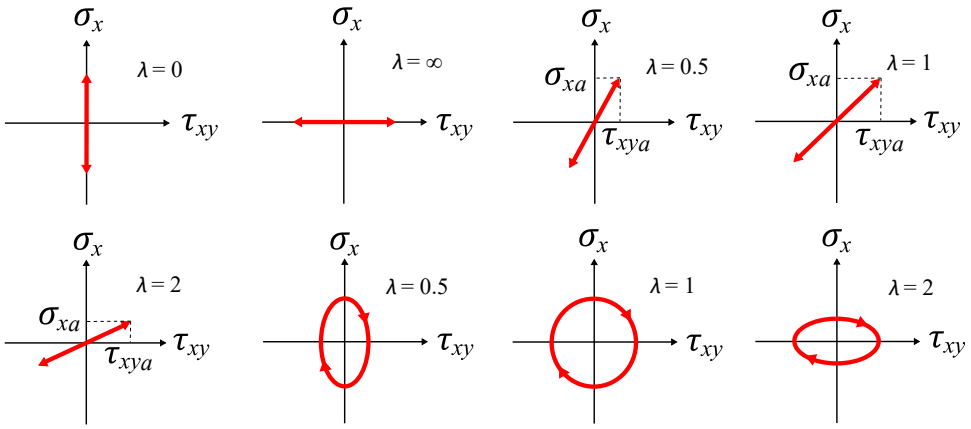

Figure 5. Stress paths used in the fatigue tests.

For axial and torsional loading, the fatigue tests were planned to provide *S-N* data of 4140 steel in the range from 5×10^4 to 2×10^6 cycles. For the in-phase and out-of-phase loading conditions, the tests were intended to obtain at least one failure and one run-out. Compared to previous works [11,28,29] on 4140 steel, the present paper has provided more data to the S-N diagram of the smooth specimen. For axial loading, replicas of the tests were made for the stress amplitudes of 484, 390, and 375 MPa. For torsional loading, replicas were also produced for the stress amplitudes of 300 and 280 MPa, as well as a new test was conducted with a stress amplitude of 250 MPa. Moreover, the S-N data for specimens with a microhole under axial and torsional loading were not presented before. These data will be discussed in Section 2.4.

Failure was defined as the complete rupture of the specimen and the tests were performed up to 2×10^6 cycles (run-out condition). The crack initiation region of the failed specimens was identified, and the direction of early crack growth (critical plane direction) was measured using a confocal laser scanning microscope.

2.3 Characterization of non-metallic inclusions

The 4140 steel has a naturally defective microstructure characterized by non-metallic inclusions. These defects are an agglomeration of contaminants that, in general, reduce the resistance of the material [7,39]. The non-metallic inclusions of the 4140 steel investigated here are shown in Fig. 6, where it is possible to observe several inclusions in a polished sample of the material.

To support the fatigue analysis that will be discussed later, a summary of the characterization and statistical analyses of defects reported earlier [11] are presented in this section. New details of the methodology (depicted in Figs. 7 and 8) are described here to help the reader understand the steps to identify and measure the size of non-metallic inclusions.

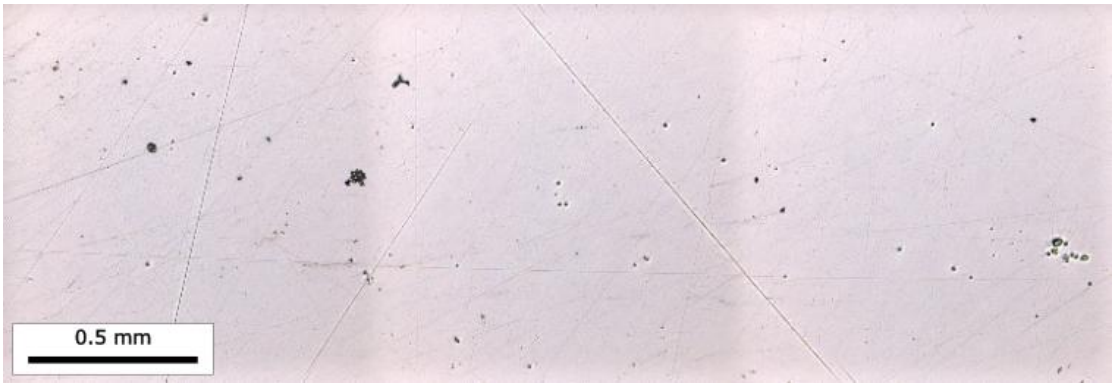

Figure 6. Non-metallic inclusions in a polished sample of 4140 steel.

The 4140 steel was analyzed in a confocal laser scanning microscope on two samples cut in two different planes (see Fig. 7): one plane at 90° and the other at 45°, relative to the longitudinal axis of the specimen. As will be discussed in Section 2.4, the 4140 steel failed predominately due to tensile crack formation in the range of fatigue lives considered in this study. Since for tensile cracking behavior, the 90º and 45º planes are

the critical planes under tension-compression and torsion, respectively, these planes were selected for metallographic analysis.

The inclusion rating of 4140 steel was determined by the method of statistics of extremes [37,40,41]. The analysis consisted of measuring the largest inclusion in each of the 60 inspection areas located at the edge of the sample, as illustrated in Fig. 7. The size S_0 of each inspection area was 0.41 mm^2. For each inspection area, the inclusion of maximum size was identified using a confocal laser scanning microscope. The square root of the projected area of this inclusion, $\sqrt{area}_{\max}$, was then calculated. Illustrations of the contours used to define the area of non-metallic inclusions are shown in Fig. 8. The distribution of $\sqrt{area}_{\max}$ over the 60 areas examined in the sample cut at 90° is given in Fig. 9, after arrangement in ascending order. For the 45° sample, a similar distribution of $\sqrt{area}_{\max}$ was observed.

Note that the distribution of $\sqrt{area}_{\max}$ is obtained in a 2D region (the cutting plane), but the inclusions are actually in a 3D region (the volume of the uniform gage of the specimen). To deal with this issue, a 3D inspection volume $V_0 = S_0 h$ was created by adding a thickness h to the inspection area S_0. The thickness is defined as the mean value of the quantities $\sqrt{area}_{\max}$. From the inspection volume V_0, the method provides the $\sqrt{area}_{\max}$ that is expected to be present in the volume V of the uniform gage of the specimen. It was found that $\sqrt{area}_{\max}$ = 145 μm in the volume V when the data from the 90º sample was considered in the analysis, and $\sqrt{area}_{\max}$ = 121 μm using the 45º sample. It should be noted that, for simplicity, the same procedure was considered in both loading conditions. Of course, this leads to a conservative estimate in the case of torsional loads, since the critical volume would in fact be a cylindrical shell with a small thickness where the stresses would be higher. For more details on the implementation of the method, the reader is referred to Ref. [11].

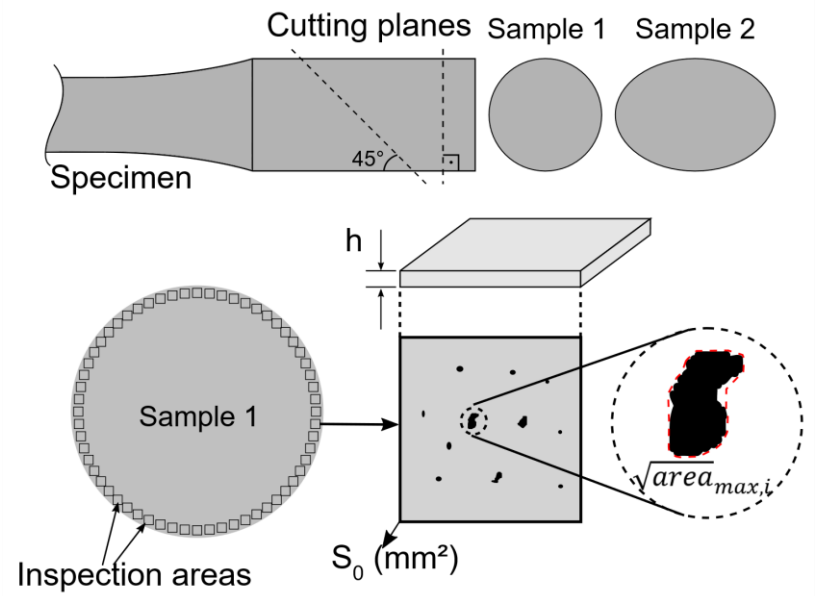

Figure 7. Procedure to measure the size of the non-metallic inclusions.

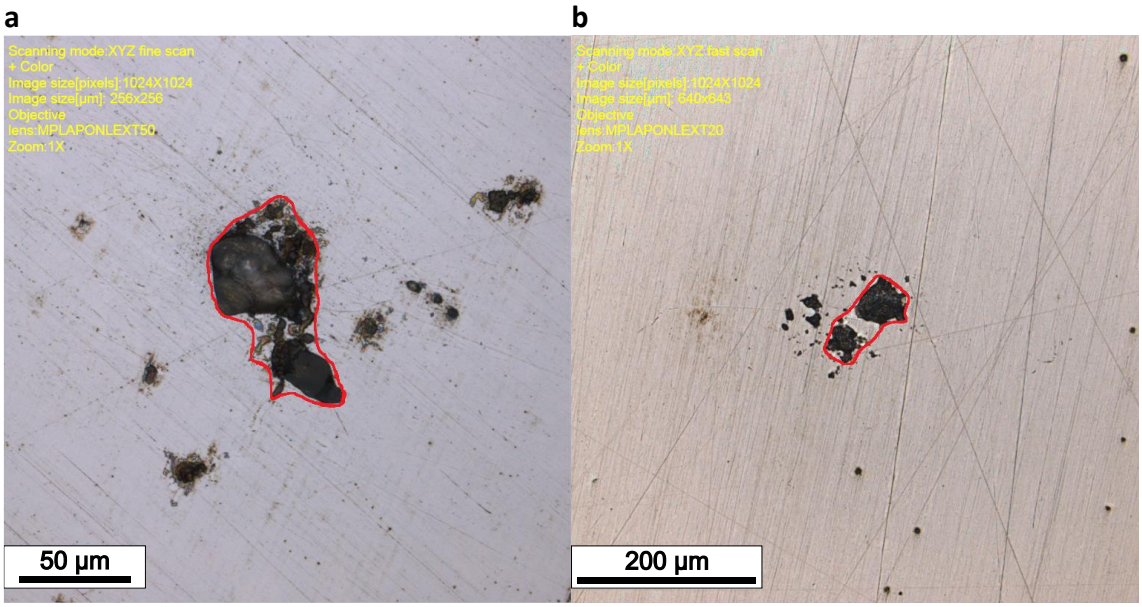

Figure 8. Illustrations of the contours used to obtain the areas of non-metallic inclusions.

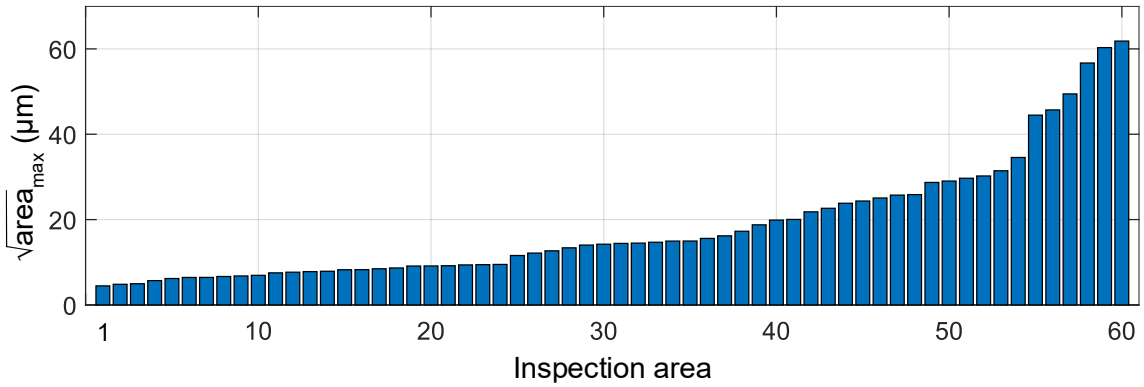

Figure 9. Square root of the projected area of the inclusion of maximum size in ascending order, for the inspection areas of the 4140 steel sample cut at 90° (refer to Fig. 7).

2.4 Fatigue criterion for small defects

A critical plane criterion for defects that fail by tensile cracking [33,34] is used in this study to predict the fatigue strength of 4140 steel. This criterion has been applied to experimental conditions involving defects with different shapes (regular and irregular), nonproportional loading, and mean/static stresses. In this section, a summary of the fatigue criterion is presented. Although the tests on 4140 steel were under fully reversed loading, the formulation is given in its general form for the sake of completeness.

Consider the representative volume element shown in Fig. 4, where σ_x and τ_{xy} are the applied axial and shear stress histories. Fatigue tests conducted on small defects [42] have shown that materials that fail by tensile crack growth are affected by the presence of biaxial stresses, a phenomenon known as the *biaxial stress effect*. To incorporate this effect in a stress-based fatigue criterion, an effective normal stress is defined by

$$\bar{\sigma}(\theta,t) = \sigma_{x'}(\theta,t) + k\sigma_{y'}(\theta,t) \tag{3}$$

where $\sigma_{x'}(\theta,t)$ and $\sigma_{y'}(\theta,t)$ are the normal stresses acting on a volume element referred to a coordinate system rotated by an angle θ around the z-axis (see Fig. 4). The constant k in Eq. (3) quantifies the sensitivity of the defect-containing volume to the biaxial stress effect.

Another important effect to be described by a fatigue criterion is the influence of mean/static stresses on fatigue strength. This effect is considered by using the Walker

parameter due to its excellent predictive capability [43]. To deal with multiaxial stress histories, the Walker parameter is applied to the effective stress given by Eq. (3), instead of its traditional use as a mean stress correction to uniaxial fatigue. Therefore, the following Walker-type fatigue parameter is defined:

$$\mathrm{FP}(\theta) = \bar{\sigma}_{\mathrm{a}}^{m} \bar{\sigma}_{\max}{}^{1-m} \tag{4}$$

where $\bar{\sigma}_{\mathrm{a}} \equiv \bar{\sigma}_{\mathrm{a}}(\theta)$ and $\bar{\sigma}_{\max} \equiv \bar{\sigma}_{\max}(\theta)$ are the amplitude and the maximum value of the time-varying effective stress $\bar{\sigma}(\theta, t)$, respectively, at a given plane defined by the angle θ. The constant m gives the sensitivity of the defect-containing volume to mean/static stress.

The critical plane is found by comparing, at each orientation θ of the volume element, the fatigue parameter $\mathrm{FP} \equiv \mathrm{FP}(\theta)$ with the uniaxial fatigue strength $\sigma_{\mathrm{w}\prime} \equiv \sigma_{\mathrm{w}\prime}(\theta)$. That is, the critical plane is defined by the maximization procedure

$$\max_{\theta}(\mathrm{FP} - \sigma_{\mathrm{w}\prime}) = 0 \tag{5}$$

Note that the fatigue strength $\sigma_{\mathrm{w}\prime}$ can in general vary with the orientation θ of the plane. This situation will occur when the defect shape is such that its projected area onto the plane perpendicular to the x'-axis is not constant over the angle θ. Also note that the critical plane search requires the calculation of the stresses associated with an arbitrary plane oriented at an angle θ. This is performed by using the well-known stress transformation formulas of Solid Mechanics [44].

The determination of the constants of the fatigue criterion is as follows. The constant k in Eq. (3) is obtained by applying the criterion to fully reversed uniaxial and torsional test data. It can be shown [33,34] that this procedure implies that

$$k = 1 - \frac{\sigma_{\mathrm{w}}}{\tau_{\mathrm{w}}} \tag{6}$$

where σ_{w} and τ_{w} are the uniaxial and torsional fatigue strengths, respectively. The constant m has to be obtained by fitting the criterion to test data involving mean stress. However, note that for the special case of fully reversed loading $\bar{\sigma}_{\max} = \bar{\sigma}_{\mathrm{m}} + \bar{\sigma}_{\mathrm{a}} = \bar{\sigma}_{\mathrm{a}}$, since the mean value of the effective stress $\bar{\sigma}_{\mathrm{m}} = 0$. The fatigue parameter is thus reduced

to FP $= \bar{\sigma}_{\mathrm{a}}$ and the constant m is not needed. This is the case of interest to the present study because all fatigue tests were conducted under fully reversed loading.

Finally, note that the fatigue criterion can be applied to metallic materials containing microstructural defects (e.g., non-metallic inclusions) as well as to macroscopic surface defects. To accomplish this, one strategy is to obtain σ_{w} and τ_{w} by fatigue testing. Alternatively, σ_{w} and τ_{w} can be calculated using formulas based on the defect size $\sqrt{area}$. For metals with natural defects in the microstructure, the expected maximum defect size $\sqrt{area}_{\max}$ has to be statistically estimated. For a macrodefect, the $\sqrt{area}$ is obtained by projecting the defect onto the plane being analyzed (i.e., the plane perpendicular to the x' direction). These two calibration procedures will be implemented and discussed in the next Section for predicting the fatigue strength of 4140 steel.

2.5 Results and discussion

2.5.1 Basic fatigue behavior

The fundamental mechanism of early fatigue crack formation can be identified by observing the response of a material to fully reversed tension-compression and torsion (pure shear) [45,46]. This physical behavior serves as a guide for selecting an appropriate fatigue damage model for a particular material. For the 4140 steel, the directions of crack growth under tension-compression and torsion are illustrated in the S-N diagrams of Figs. 10 and 11, respectively for the material in plain condition and with a blind microhole.

The volume element in these figures represents a small portion of material with characteristic length in the millimeter scale. Moreover, the crack direction illustrated in the volume element gives the overall (average) orientation of a crack in its early stage. This engineering approach is consistent with the bulk nature of the fatigue parameter used in our analysis, which was formulated using the macroscopic stress as input. Note that for a description of the intricate path of a small fatigue crack, the crystallographic texture of the material would have to be included in the model. For further discussions on continuum-based and microstructure-sensitive approaches to fatigue, see [46–48].

Figure 12 shows regions on the surface of the specimens where crack formation occurred. The images were obtained with a confocal microscope, and the crack orientation angles were measured with the microscope's software which allows measuring

the inclination of the fatigue fracture surface. The observation of the crack directions of 4140 steel under tension-compression (Fig. 10(a) and 12(a)) revealed critical planes consistently perpendicular to the specimen axis. For cyclic shear stress at an amplitude of 320 MPa, which resulted in lives around 2×10^5 cycles, the normal to the critical plane was ±45º with respect to the specimen axis, as depicted in Figs. 11(b) and 12(b).

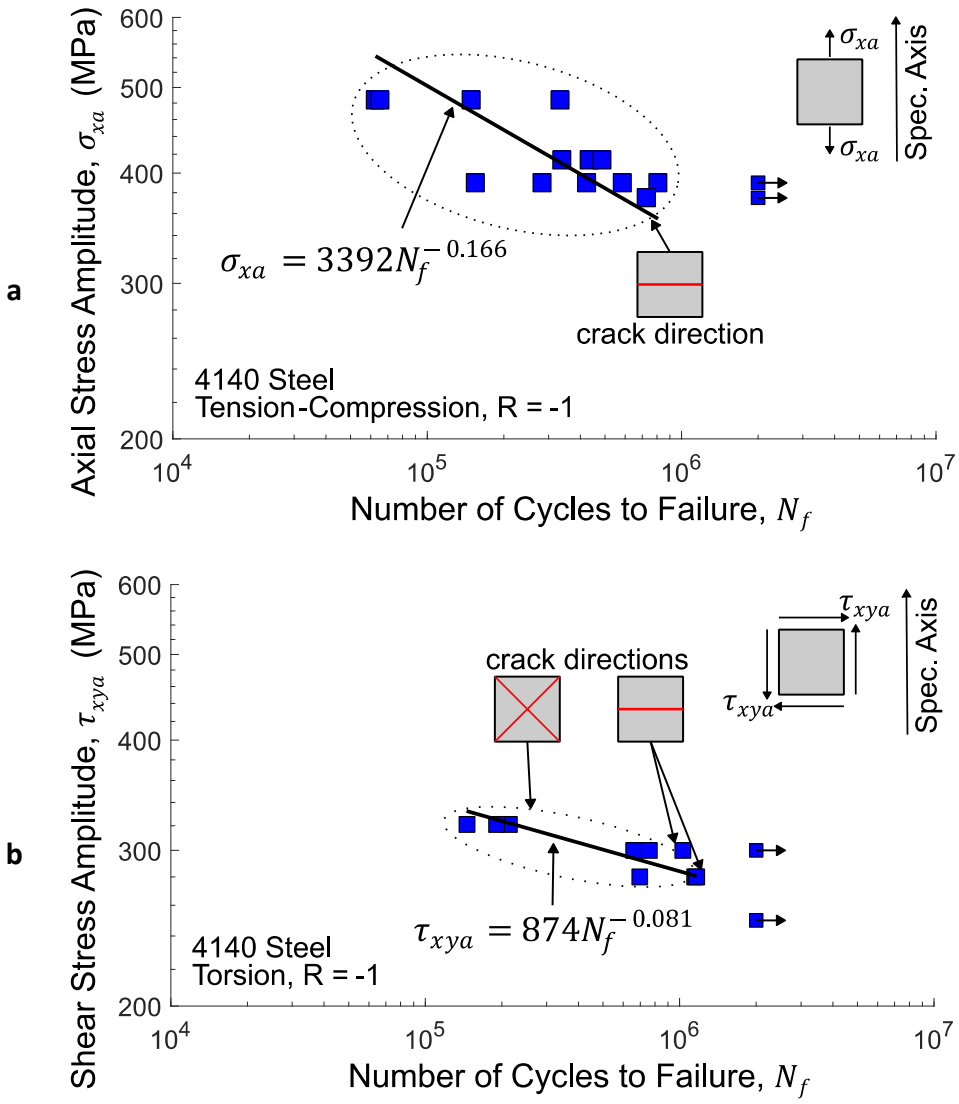

Figure 10. Fatigue lives and crack directions of 4140 steel for (a) tension-compression and (b) torsion.

However, for the six tests conducted at lower shear stress amplitudes of 300 and 280 MPa (lives around 106 cycles) an irregular pattern of crack formation occurred in which both 0º and 45º oriented critical planes were observed at the same loading amplitude (see Fig. 10(b)). More specifically, four failures occurred with 45º oriented

critical planes, and two with 0º oriented critical planes. Observation of the fracture surfaces of these specimens suggested the occurrence of subsurface crack initiation in a non-metallic inclusion. However, due to the rubbing of the fracture surfaces due to torsion loading, confirmation of this hypothesis was not possible.

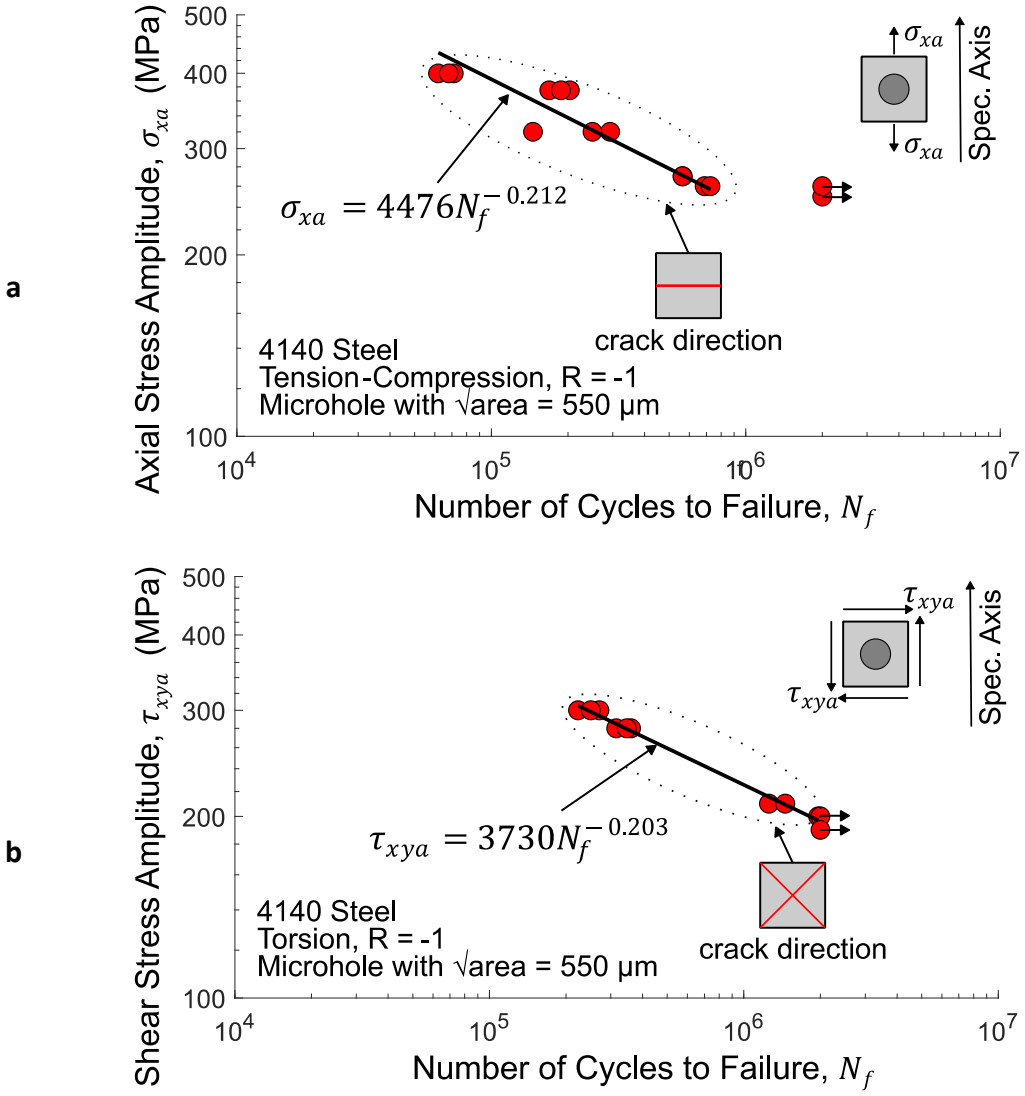

Figure 11. Fatigue lives and crack directions of 4140 steel with a microhole for (a) tension-compression and (b) torsion.

The basic cracking behavior of 4140 steel with a superficial microhole is shown in Figs. 11(a) and 11(b), respectively for tension-compression and torsion loading. Fig. 12(c-d) shows images of the crack orientation in relation to the microhole for these loads. In both situations, the fatigue cracks were consistently formed along the planes with maximum normal stress amplitude. From the crack directions shown in Figs. 10, 11, and

15, it can be concluded that the cracking behavior of 4140 steel is mainly dominated by tensile crack growth in the range of fatigue lives investigated. This behavior justifies the use of the normal stress-based fatigue criterion presented in Section 2.3, which predicts tensile cracks under tension-compression and torsion.

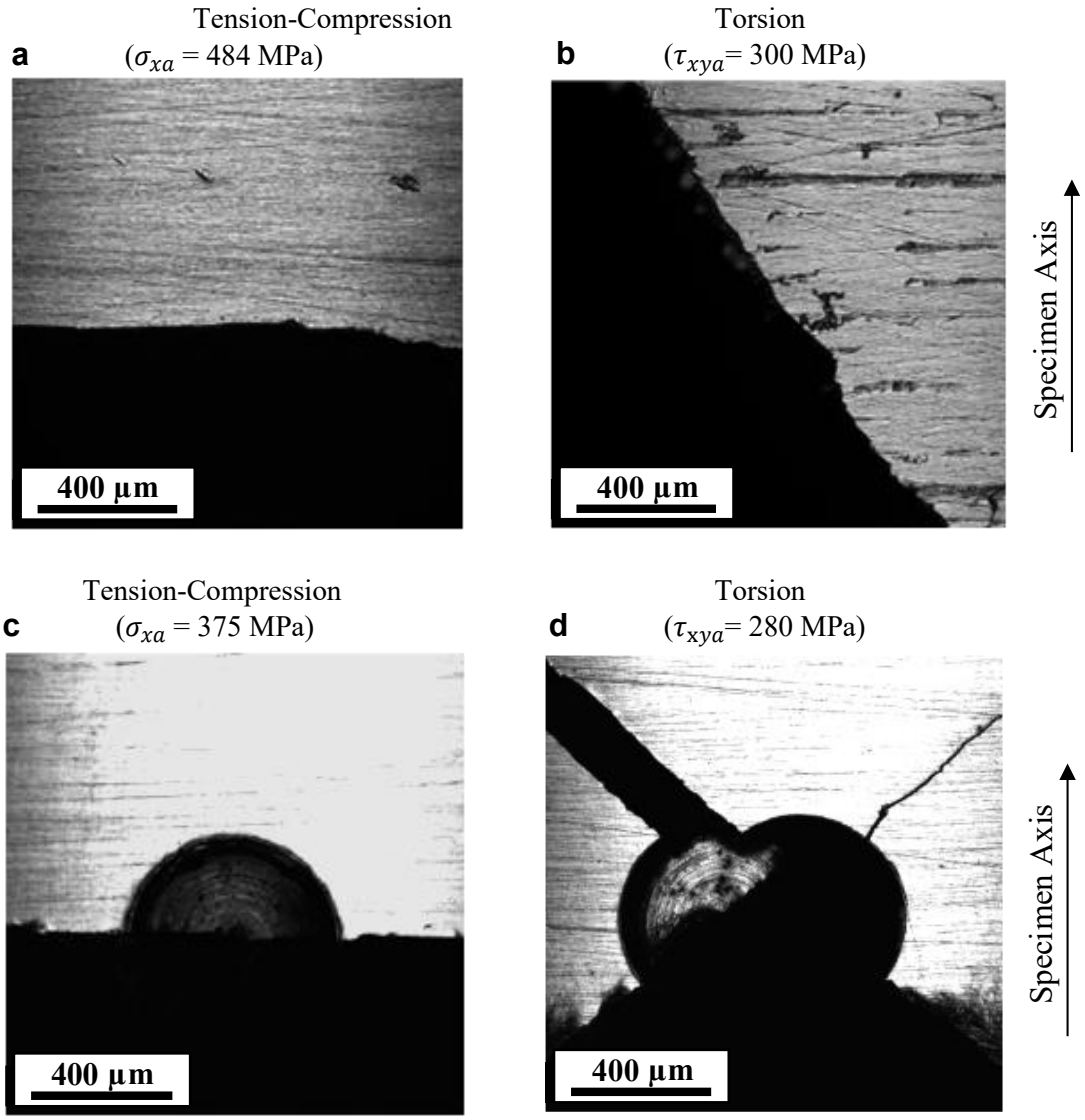

Figure 12. Observed fatigue crack orientations: (a) plain specimen in tension-compression, (b) plain specimen in torsion, (c) specimen with microhole in tension-compression, and (d) specimen with microhole in torsion.

2.5.2 Evaluation of fatigue strength predictions

To evaluate the predictions made using the fatigue parameter, Eq. (4), the following performance indicator was adopted:

$$\text{Error} = \frac{\text{FP}-\sigma_{\text{w}}}{\sigma_{\text{w}}}\ (\%) \tag{7}$$

where the fatigue parameter FP is calculated using the experimental fatigue strengths and σ_{w} is the uniaxial fatigue strength. As this error indicator is frequently used in evaluations of fatigue criteria [49–51], it allows us to compare the errors obtained in the present study with those obtained in studies involving "defect-free" materials.

Note that the calculation of FP requires the value of k (see Eqs. (3) and (4)) which, by its turn, is given by $k = 1 - \sigma_{\text{w}}/\tau_{\text{w}}$. Consequently, the error indicator will depend on the values of the uniaxial fatigue strength σ_{w} and torsional fatigue strength τ_{w}. Two calibration procedures, labeled A and B, were used to obtain these constants. In calibration A, the uniaxial and torsional fatigue strengths were estimated using relations based on the $\sqrt{area}$ approach [2,11,19]. Calibration B considered the uniaxial and torsional fatigue strengths obtained experimentally.

The relations based on the $\sqrt{area}$ parameter to estimate the fatigue strengths are given by Eqs. (8) and (9), where $\sqrt{area}_{\text{max}}$ is a value calculated by statistics of the extrema of the largest inclusion expected to be found in the gage region of the specimen. Eqs. (8) and (9) estimate the lower bound fatigue strengths considering the effect of the non-metallic inclusions in the material, where 1.41 and 1.19 represent factors of adjustment regarding subsurface defects, which are considered to be the most detrimental [2,11].

$$\sigma_{\text{w}} = \frac{1.41(HV+120)}{(\sqrt{area}_{\text{max}})^{1/6}} \tag{8}$$

$$\tau_{\text{w}} = \frac{1.19(HV+120)}{(\sqrt{area}_{\text{max}})^{1/6}} \tag{9}$$

Moreover, Eqs. (10) and (11) consider the $\sqrt{area}$ of a small (but macroscopically visible) surface defect, where, in this case, the values 1.43 and 1.21 are adjustment factors for these types of defects [2,19].

$$\sigma_{\text{w}} = \frac{1.43(HV+120)}{(\sqrt{area})^{1/6}} \tag{10}$$

$$\tau_{\text{w}} = \frac{1.21(HV+120)}{(\sqrt{area})^{1/6}} \tag{11}$$

The Vickers hardness (HV) of the 4140 steel is 320 kgf/mm^2. For the plain specimens, only with its own non-metallic inclusions, the square root of the largest inclusions was estimated through the extreme statistics method as described in Section 2.2. This procedure resulted in $\sigma_w = 271$ MPa and τ_w = 235 MPa, which implied that $k = -0.15$. In calibration B for the plain specimens, the fatigue strength was calculated by extrapolating the S-N curves up to 2×10^6. The obtained values of the uniaxial and torsional fatigue strengths were $\sigma_w = 305$ MPa and τ_w = 269 MPa, hence, $k = -0.13$.

To calculate the fatigue strength in the presence of the microhole it was only necessary to calculate its projected area in the direction of the maximum principal stress in tension and torsion. The projection of the hole forms a square with sides equal to the diameter of the hole in both directions, therefore the computed value of $\sqrt{area}$ was $550\ \mu m$. This led to $\sigma_w = 220$ MPa and τ_w = 186 MPa, which implies that $k = -0.18$. While in calibration B, for the specimens with microhole, $k = -0.06$ and the fatigue strengths at 2×10^6 cycles were $\sigma_w = 207$ MPa and τ_w = 196MPa).

Table 3. Experimental fatigue strengths of 4140 steel at $\mathbf{2 \times 10^6}$ cycles.

Test ID	Loading type	Plain specimen		Specimen with microhole	
		σ_{xa} (MPa)	τ_{xya} (MPa)	σ_{xa} (MPa)	τ_{xya} (MPa)
1	Axial, $\lambda = 0$	305	0	207	0
2	Torsional, $\lambda = \infty$	0	269	0	196
3	In-phase, $\lambda = 1$	200	200	150	150
4	In-phase, $\lambda = 0.5$	280	140	200	100
5	In-phase, $\lambda = 2$	120	240	90	180
6	90° Out-of-phase, $\lambda = 1$	220	220	180	180
7	90° Out-of-phase, $\lambda = 0.5$	300	150	230	115
8	90° Out-of-phase, $\lambda = 2$	135	270	100	200

The fatigue strengths under the combined loading conditions were defined as the first stress level at which failure was not observed. All the fatigue strengths adopted in calibration B are presented in Table 3.

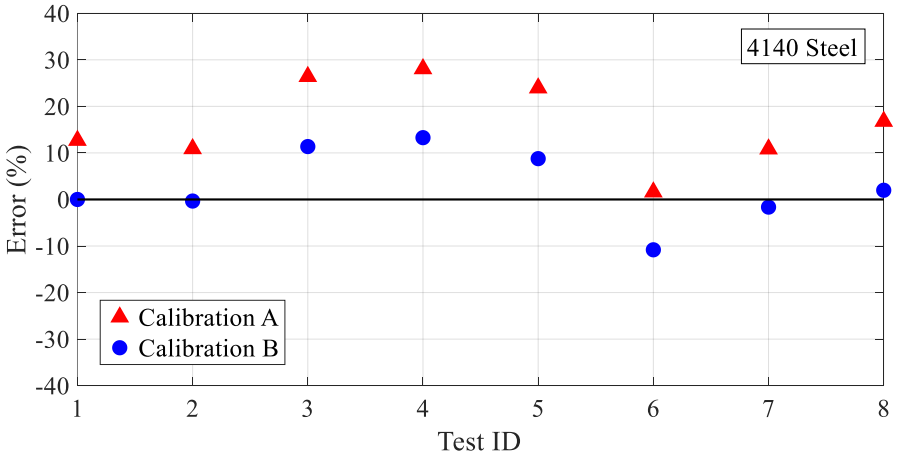

Figure 13. Errors of the predicted fatigue strengths of plain 4140 steel.

The errors of the predicted fatigue strengths of plain 4140 steel are shown in Fig. 13. Calibration A resulted in errors from 1.6 to 28.1%, while Calibration B yielded errors in the range of -10.8 to 13.3%. The higher errors obtained by using Calibration A can be attributed to the inaccuracy of relations (8) and (9) in estimating the uniaxial and torsional fatigue strengths of 4140 steel. The accuracy of the predictions based on Calibration B was comparable to those typically observed in evaluations of fatigue criteria [52,53]. The errors of the predicted fatigue strengths of 4140 steel with microhole are shown in Fig. 14. Calibration A resulted in errors from -5.8 to 18.0%, while Calibration B yielded errors in the range of 0.0 to 19.9%.

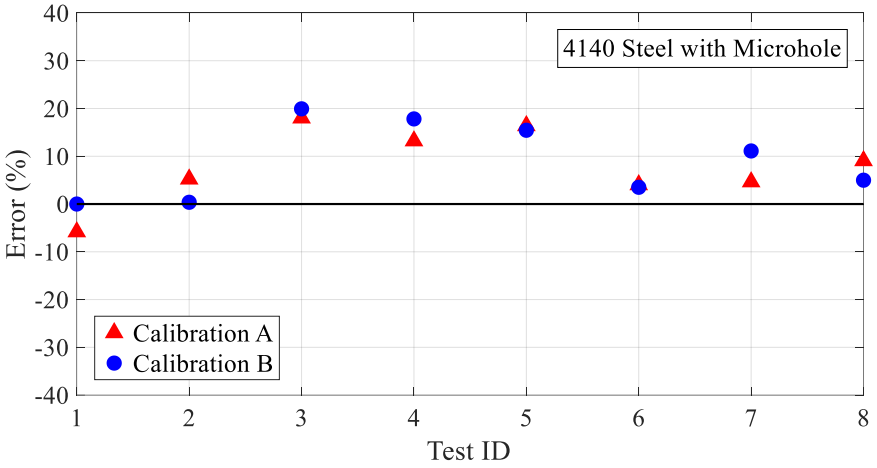

Figure 14. Errors of the predicted fatigue strengths of 4140 steel with a microhole.

The conservativeness of calibration A for the case of plain specimens may be associated with the maximum inclusion square root of area predictions, from which the lower bound of the fatigue strengths are defined. These inclusions may or may not exist in the analyzed specimen, which generates a lot of scatter in the fatigue results, as can be observed in the S-N curves of the plain specimens (Fig. 11). However, the use of this approach enhances the safety due to the conservatism of the predictions.

2.5.3 Evaluation of critical plane orientations

Since fatigue cracks have a directional nature, an appropriate fatigue damage model should predict fatigue strengths well, for a variety of loading conditions and also properly predict the physically observed directional damage. In practical terms, predicted critical plane angles should agree with measured crack angles.

In Figs. 15 and 16, the crack angles measured at the plain specimens and at the specimens with microhole are represented by red ‘x’ symbols for each failed test specimen. The fatigue parameter was normalized so that its maximum value is equal to one. The solid blue lines represent the range of predicted crack angles when the fatigue parameter is between 90% and 100% of its maximum value. The estimated and observed crack angles are in good agreement for almost all loading cases. In the case of plain specimens some data are slightly above or below the predicted range (Fig.15). It is remarkable that for the specimens with microhole the estimates of the critical plane angles are very accurate (see Fig.16).

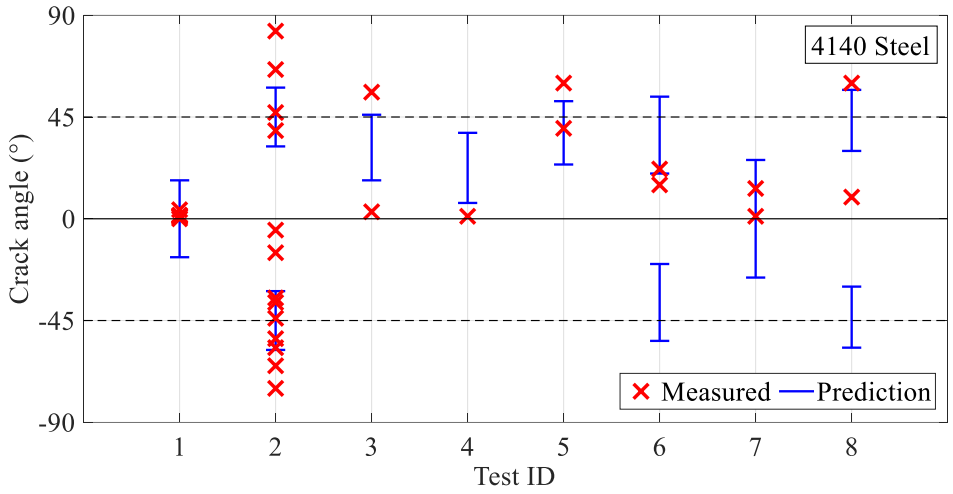

Figure 15. Predicted and measured crack angles for plain specimens.

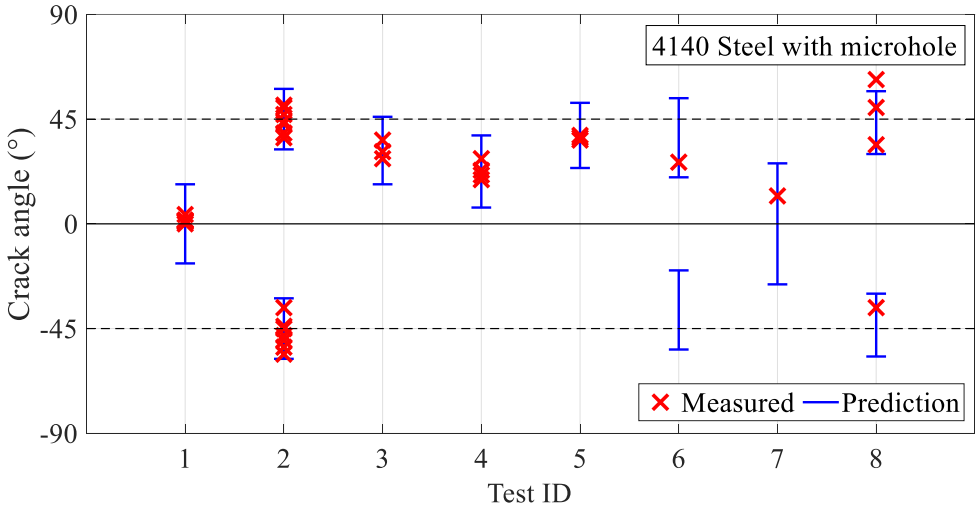

Figure 16. Predicted and measured crack angles for specimens with microhole.

2.6 Conclusions

High-cycle fatigue test data of 4140 steel under fully reversed axial, torsional, and combined axial and torsional (in-phase and out-of-phase) loading were investigated in this paper. The tests were made on plain specimens containing only their inherent non-metallic inclusions and on specimens with a small blind hole milled into the surface. The following conclusions were drawn from this work:

I. For the specimens with a small surface hole, fatigue cracks were consistently formed along the planes with maximum normal stress amplitude (tensile failure

mode). For most of the plain specimens, tensile-driven small cracks were also observed.

II. For plain specimens under torsional loading, at fatigue lives around 10^6 cycles, both tensile and shear cracks were observed in tests replicated at the same loading amplitude. This result shows the complexity of fatigue crack formation in 4140 steel and poses a difficulty for any fatigue modelling approach.

III. Predictions of fatigue strength and crack direction were satisfactory for engineering purposes, both for the plain specimens and the specimens with a small surface hole. These predictions were calculated using a critical plane fatigue criterion that incorporates the $\sqrt{area}$ parameter to quantify the defect size. For the plain specimens, the maximum size of the non-metallic inclusions was estimated by the method of statistics of extremes. For the specimens with a surface hole, the defect size was obtained by projecting the hole onto the plane under analysis.

3. A NEW MULTIAXIAL FATIGUE ENDURANCE MODEL FOR HIGH STRENGTH STEELS TAKING INTO ACCOUNT THE PRESENCE OF SMALL DEFECTS

This chapter is a reproduction of the following publication:

- Araujo LC, Malcher L, de Oliveira D, Araújo JA. A new multiaxial fatigue endurance model for high strength steels taking into account the presence of small defects. International Journal of Fatigue 2024;178

Abstract

In the present work, a new multiaxial fatigue model is proposed for metallic material with small defects. This model correlates the uniaxial fatigue limit obtained from the $\sqrt{area}$ parameter of a high strength steel containing small defects with values associated with the amplitude of the principal stresses, whose calculation for non-proportional loadings is not trivial. The performance of the model was evaluated with experimental data from AISI 4140 steel, under various loading conditions, in which smooth cylindrical bars were considered, regarding: (i) the effect of non-metallic inclusions in the material, and (ii) superficial micro hole with a straight bottom machined in the material (550 μm in diameter and depth). The proposed model has provided accurate fatigue strength estimates with average error not exceeding 16%.

Keywords: Multiaxial fatigue; small defects; $\sqrt{area}$ parameter; principal stress amplitude.

3.1 Introduction

The influence of small defects on the fatigue strength of metallic materials has been the object of study by several researchers over the last decades [1,2,16,54]. One of the models that address the problem and that has been standing out over the years is the $\sqrt{area}$ parameter, proposed by Murakami [2], as well as its variations and adaptations proposed by other researchers [1,2,40,55]. However, the models based on the $\sqrt{area}$ parameter have been widely applied under uniaxial fatigue. More recently, some works

have been developed addressing the fatigue problem in the presence of small defects with more complex loading conditions [8,11,18–21,28,31,56–59]. The importance of this type of study is justified by the frequent presence of multiaxial stress states in real engineering components, due to either geometric factors of the component and/or multiple combined loads.

As an example, fatigue failures due to the presence of non-metallic inclusions in crankshafts of thermo generators in Brazilian plants have been recently reported. These crankshafts are made of high strength steels, AISI 4140 (DIN 42CrMo4) or AISI 4340 (DIN 34CrNiMo6), forged and heat treated. High strength steels are used in a wide range of engineering components and it has been observed that in this type of material, fatigue failures generally originate in non-metallic inclusions [11,60–64]. Therefore, it seems to be necessary the existence of multiaxial fatigue strength criteria that consider non-metallic inclusions or small defects.

In this work, a new multiaxial fatigue model proposed by the authors is presented, which relates the fatigue limit of the material obtained from the $\sqrt{area}$ parameter with values associated with the principal stresses generated by the loads. These values are the amplitude of the principal stresses and the maximum value in time of the greatest principal stress. The computation of these variables is not a trivial task as, under non-proportional multiaxial loads, not only the value, but the directions of the principal stresses vary from instant to instant. Therefore, mainly the calculation of the principal stresses amplitude posed a challenge that had not yet been addressed by other researchers, to the best of the authors' knowledge.

To evaluate the proposed model, new experimental data under uniaxial and under combined loading (tension/torsion in-phase and out-of-phase) were generated considering not only smooth naturally defective cylindrical specimens made of AISI 4140 steel, but also specimens with an artificial micro hole. Additionally, data previously produced by the authors with this same material and already available in the literature were added to the analysis.

3.2 Fatigue Strength Estimation from $\sqrt{area}$ Parameter

Based on fracture mechanics theories and on experimental observations with specimens of different materials and with different types of small defects (such as small

drilled holes, very small and shallow notches, and very shallow circumferential cracks), the $\sqrt{area}$ parameter model proposed by Murakami and Endo [2,16] is an empirical correlation to estimate the fatigue limit, defined as the threshold condition for non-propagation of cracks emanating from the small defects at 10^7 cycles. This model can be applied to small defects or cracks within a certain range of $\sqrt{area}$ values. The upper limit of $\sqrt{area}$ for these equations is not yet definitively established, but it seems to be around 1000 μm. On the other hand, the lower limit of applicability varies depending on material properties and microstructures.

One of the advantages of $\sqrt{area}$ parameter proposed by Murakami is that one can obtain the fatigue strength for materials with micro defects, σ_w, without the need to carry out fatigue tests. Regarding superficial defects of known size and shape, the square root of the defect's projected area ($\sqrt{area}$) and the material hardness (Hv) in Vickers are required, how is represented by Eq. (12):

$$\sigma_w = \frac{1.43(Hv+120)}{(\sqrt{area})^{1/6}} \tag{12}$$

where σ_w represents the fatigue limit for materials with micro defects [MPa], Hv is the Vickers hardness [kgf/mm^2] and $\sqrt{area}$ is represented in [μm]. The values 1.43 and 120 represent factors of adjustment regarding superficial defects. Moreover, the plane to which the defect's area is projected is normal to the greatest principal stress direction under uniaxial loading.

However, to determine the area of internal defects, such as non-metallic inclusions or pores, which can exist in large quantities and with different sizes and shapes, it is necessary to conduct a statistical analysis to determine what is the likely largest existing defect in function of the volume of material. This likely biggest defect is denominated, $\sqrt{area}_{max}$ [2,37,65].

Murakami considers that the most detrimental type of internal defect was the one just in contact with the free surface [2]. When a crack nucleates around this type of defect, it usually grows and occupies all the weak area between the defect and the free surface. This 'extra' area needs to be considered in the calculation of the $\sqrt{area}$. To do so, the lower bound of the uniaxial fatigue limit was dined as follows:

$$\sigma_w = \frac{1.41(Hv+120)}{(\sqrt{area}_{max})^{1/6}} \quad (13)$$

where the values 1.41 and 120 represent factors of adjustment regarding subsurface defects. The dimension of each parameter of Eq. (13) follows Eq. (12).

3.3 Multiaxial Model Proposal

In studies available in the literature with combined loads, it was observed that, in the fatigue limit condition, short non-propagated cracks can be seen emanating from small defects [8,17,39]. The direction of these cracks has been reported to be approximately perpendicular to the direction of the maximum principal stress. Therefore, some models were proposed that related the fatigue limit with values associated with the principal stresses [8,17,66].

Different from existing models so far, which use instantaneous values of the combination of principal stresses to compute the fatigue damage [8,17,66] the new model here proposed will consider the amplitude value associated with the principal stresses as one of its governing variables. As a matter of fact, the proposed model can be considered as a modification of the celebrated Smith, Watson, and Topper (SWT) Parameter [67,68], and can be written as:

$$\mathrm{SWT}_{\mathrm{mod}} = \sqrt{\sigma_{p,max}\sigma_{p,a}} \quad (14)$$

where $\mathrm{SWT}_{\mathrm{mod}}$ represents the Modified Smith, Watson and Topper parameter, $\sigma_{p,max}$ is the maximum value of the greatest principal stress at any time instant during the loading cycle and $\sigma_{p,a}$ is the amplitude of the principal stresses. As mentioned before, the computation of such amplitude value is not trivial and will be described in more details further down. This relationship has the advantage of not relying on any material constant. At last, a mechanical component containing a small defect subjected to a loading history will be considered safe if the following inequality holds:

$$\mathrm{SWT}_{\mathrm{mod}} \leq \sigma_w \quad (15)$$

where the fatigue parameter, SWT_{mod}, are obtained from Eq. (14) and the uniaxial fatigue limit, σ_w, from the $\sqrt{area}$ parameter is obtained from Eq. (12) or Eq. (13).

3.3.1 Principal stresses amplitude

Consider the following combined loading history:

$$\sigma_x = \sigma_{xa} \sin \omega t \tag{16}$$

$$\tau_{xy} = \tau_{xya} \sin(\omega t + \delta) \tag{17}$$

where σ_{xa} and τ_{xya} are the amplitudes of the normal and shear stresses respectively, ω is the angular frequency, t is time and δ is the phase angle between the loads. For each instant of time, the maximum and minimum principal stresses and their directions can be easily obtained by the eigenvalues and eigenvectors of the Cauchy stress tensor [68]. With a cyclic loading history, each principal stress vector, $\boldsymbol{\sigma_{p,max}}$ and $\boldsymbol{\sigma_{p,min}}$, will describe a closed path. By plotting both the paths described by the principal stress vectors and applying the Maximum Rectangular Hull method (MRH) [69] it is possible to compute the amplitude of the principal stresses, $\sigma_{p,a}$. Here, it is important to notice that the Maximum Rectangular Hull approach can also be used to compute the principal stresses amplitude even for loading cases resulting in three non-zero principal stresses varying with time.

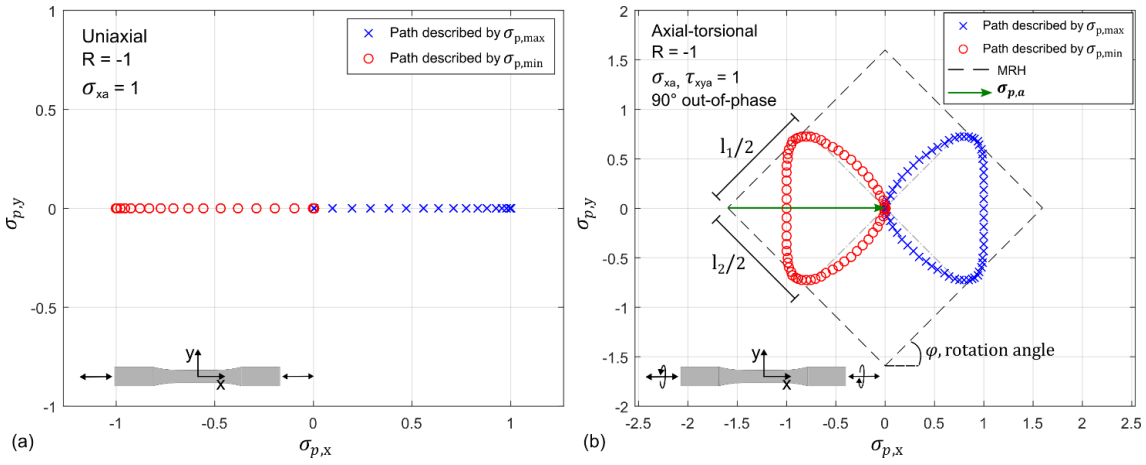

Figure 17. Path described by the principal stresses in two loading conditions: (a) traction-compression and (b) combined out-of-phase loading with application of the MRH to calculate $\sigma_{p,a}$.

Originally proposed to calculate the shear stress amplitude, the MRH method is simple to implement, and it can consider the effect of non-proportional stress histories. In the MRH, the amplitude is defined as half of the diagonal of the maximum rectangular hull that envelops the entire stress path. Fig. 17 depicts a representation of the path described by the maximum and minimum principal stresses in two different loading conditions, where $\sigma_{p,x}$ and $\sigma_{p,y}$ are the components of principal stresses projected in the x and y directions.

In Fig. 17(a) it can be seen that for uniaxial loading the path described by the maximum and minimum principal stresses form a straight line, in this particular case the value of $\sigma_{p,a}$ can be easily obtained. On the other hand, for torsional and combined axial-torsional loads, the directions of the maximum and minimum principal stress can vary greatly, as shown in Fig. 17(b) that depicts a combined out-of-phase loading and a schematic representation of the MRH method for calculation of the $\sigma_{p,a}$.

3.4 Experimental work

3.4.1 Material and fatigue specimens

The experimental campaign conducted in a previous work by the authors [11] and the new data generated for this work were obtained with fatigue specimens made of AISI 4140 steel, oil quenched and tempered in the 530 - 630 °C range, with mechanical properties reported in Table 4. The material was removed from crankshafts of thermoelectric generators that failed due to fatigue during operation.

It is important to notice that this type of crankshaft is a very large component, measuring 7 meters in length. The material to fabricate the specimens was extracted from a region distant from the critical area where cracks that caused the component failure originated. Despite the lower stress levels in the region from which the specimens were obtained, as the crankshaft endured many cycles before breaking, some level of fatigue damage may have accumulated in the material, although no small cracks were detected in the specimens. In view of this, the residual fatigue damage was considered negligible.

The specimen manufacturing process consisted of cutting the material into prisms, followed by machining to the final geometry and a polishing process to achieve

roughness less than 0.2 µm. These specimens were designed according to ASTM E466-15 with the "dog-bone" geometry, as shown in Figure 18.

Table 4. Mechanical properties of AISI 4140 steel.

Yield Strength (MPa)	Tensile Strength (MPa)	Elongation (%)	Vickers hardness (kgf/mm²)
647	932	20	320

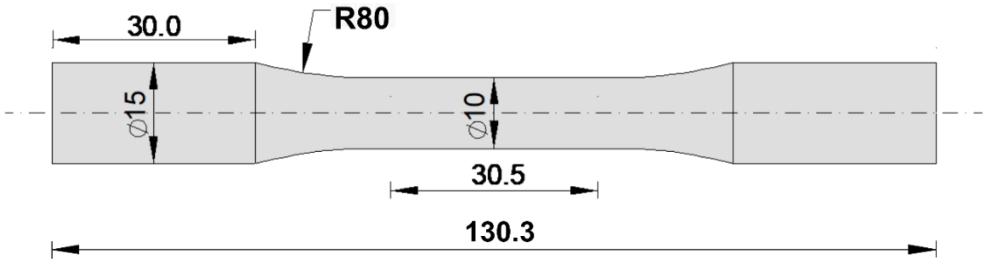

Figure 18. Specimen's geometry (dimensions in mm).

Two types of specimens were used in this experimental campaign: (i) smooth cylindrical bar specimens, without artificially introduced surface defects and (ii) specimens containing a 550 µm diameter and depth micro surface hole with a straight bottom. The geometry of the micro hole can be seen in
Figure 19.

The machining was performed in a CNC XH7132, with 3 axis and positioning resolution of 15 µm. To achieve the straight bottom, helical hole milling was preferable than micro drilling. This process is also preferable because it lowers cutting forces and produces higher surface quality than mechanical drilling [70]. In this sense, the selected tool was a WC micro end mill coated with TiAlN whit 500 µm diameter.

The cutting parameters were selected based on the literature [71,72] and improved in preliminary micro milling trials, resulting in a cutting velocity of 9,4 m/min, feed per tooth of 3,3 µm and a depth setting of the helical course of 25 µm.

During the micro milling procedure, cutting fluid was used to achieve a better finish on the micro hole surfaces. Considering that the literature reports that dry micro milling or insufficient cutting fluid can lead to lower quality, higher surface roughness

values, and adherence of material burr formation [73] synthetic cutting fluid Bio100e was diluted in water in a 1:9 ratio and applied at a flow rate of 6.0 l/min to ensure that the cut occurred submerged or in a near-submerged method, which increased the integrity of the specimens [74]. Despite all the care taken, as described above, to minimize residual stresses, we cannot deny that they exist, but they were not considered in the analysis of this work.

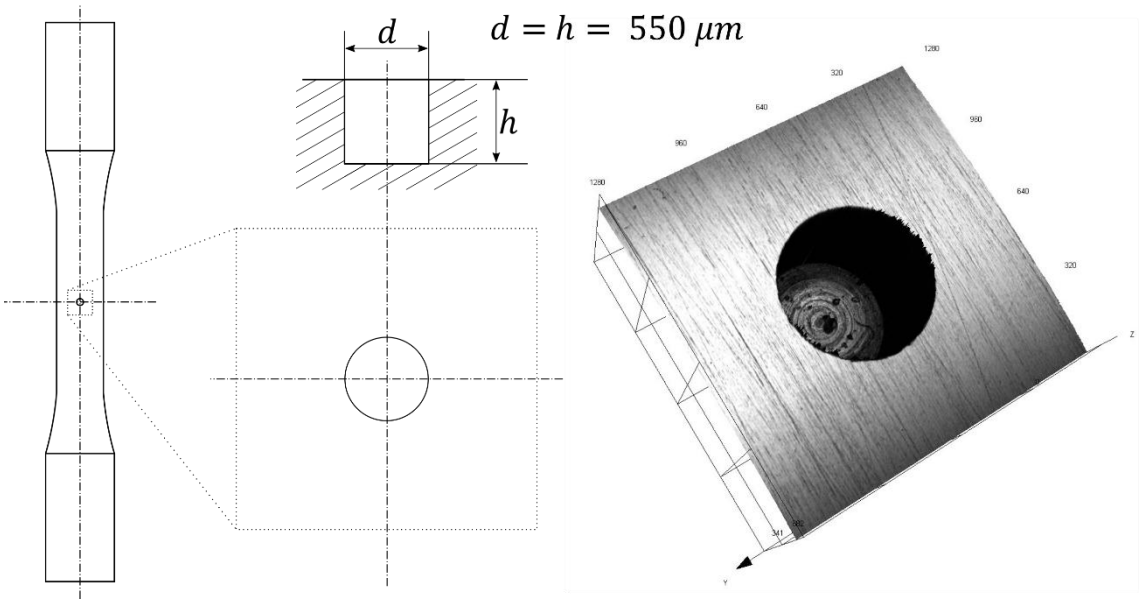

Figure 19. Micro hole produced in fatigue specimens.

3.4.2 Multiaxial Fatigue Testing

Fatigue tests were performed under force control in accordance with ASTM E466-15 in an axial (100 kN capacity) and an axial-torsional ($100\ kN$ e $1100\ Nm$) servo-hydraulic fatigue testing machines Fig. 20. During the tests, the ambient temperature was controlled and kept between 20 to 26 °C and the frequencies kept between 5 and 15 Hz, depending on the load level. All tests were carried out with totally alternating sine waves, that is, with a loading ratio R of -1.

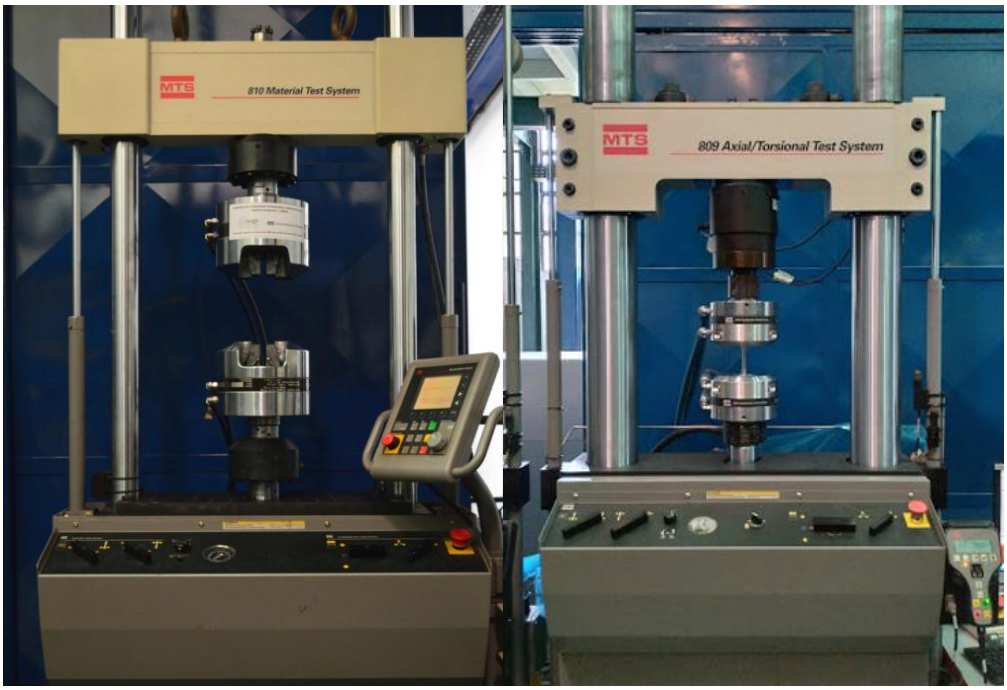

Figure 20. Fatigue Testing Machines, MTS - 810 Material test system on the left and MTS - 809 Axial/torsional test system on the right.

Fatigue tests were performed considering different ratios between shear stress amplitudes τ_{xya} and normal stress amplitudes σ_{xa} corresponding to 0, 0.5, 1, 2 and ∞, where the values of 0 and ∞ correspond to traction-compression and pure torsion loading, respectively. The other values represent combined loads, where in-phase and 90º out-of-phase tests were performed.

The objective in carrying out the tests was to obtain at least one failure and one run-out for each of the different types of loading. In these cases, the number of cycles established as stopping criterion/run-out was equal to 2×10^6 cycles, and the complete rupture of the specimen was used as a failure criterion.

Assuming a specimen failed, the stress level was reduced in the next test. On the other hand, if the run-out was reached, the next test would be performed at an incrementally higher stress level with a new specimen, that is, in the evaluation of the proposed multiaxial model, no specimen was reused.

Table 5. Test data of smooth specimens.

	Test	σ_{xa}	τ_{xya}	$\frac{\tau_{xya}}{\sigma_{xa}}$	Cycles
Uniaxial and combined in-phase	1	414	0	0	486296
	2	390	0	0	run-out
	3	390	0	0	584601
	4	375	0	0	726900
	5	375	0	0	run-out
	6	300	150	0.5	1649870
	7	300	150	0.5	run-out
	8	280	140	0.5	run-out
	9	260	130	0.5	run-out
	10	220	220	1	332449
	11	220	220	1	1363493
	12	210	210	1	run-out
	13	210	210	1	477573
	14	200	200	1	run-out
	15	130	260	2	535059
	16	130	260	2	535304
	17	120	240	2	run-out
	18	120	240	2	run-out
	19	0	320	inf	213990
	20	0	300	inf	660321
	21	0	300	inf	run-out
	22	0	280	inf	1166978
	23	0	230	inf	run-out
Combined 90° out-of-phase	1	320	160	0.5	750695
	2	320	160	0.5	352444
	3	300	150	0.5	run-out
	4	300	150	0.5	733995
	5	230	230	1	771198
	6	230	230	1	1649979
	7	220	220	1	run-out
	8	210	210	1	run-out
	9	200	200	1	run-out
	10	140	280	2	1039328
	11	140	280	2	261442
	12	135	270	2	run-out
	13	130	260	2	run-out

Table 6. Test data of specimens with a 550 μm microhole.

	Test	σ_{xa}	τ_{xya}	$\frac{\tau_{xya}}{\sigma_{xa}}$	Cycles
Uniaxial and combined in-phase	1	260	0	0	725825
	2	260	0	0	run-out
	3	250	0	0	run-out
	4	210	105	0.5	1579783
	5	210	105	0.5	1704314
	6	200	100	0.5	run-out
	7	200	100	0.5	run-out
	8	160	160	1	1502701
	9	160	160	1	1027043
	10	150	150	1	run-out
	11	150	150	1	run-out
	12	95	190	2	818412
	13	95	190	2	1330195
	14	90	180	2	run-out
	15	90	180	2	run-out
	16	0	200	inf	run-out
	17	0	200	inf	1959328
	18	0	190	inf	run-out
Combined 90° out-of-phase	1	230	115	0.5	run-out
	2	230	115	0.5	run-out
	3	240	120	0.5	717224
	4	160	160	1	run-out
	5	170	170	1	run-out
	6	170	170	1	run-out
	7	180	180	1	run-out
	8	190	190	1	936993
	9	100	200	2	run-out
	10	100	200	2	run-out
	11	105	210	2	1317786

Tables 5 and 6 contain details of the tests performed with both, smooth specimens and specimens with a 550 μm microhole, respectively. They report the loading amplitudes, ratio between shear stress and normal stress, and the number of cycles reached.

3.5 Results and Discussion

3.5.1 Fatigue limits from $\sqrt{\boldsymbol{area}}$ parameter

From the analysis of inclusions and the extreme statistics method, conducted in our previous work [11], the computed value of $\sqrt{area}_{max}$ was $145\ \mu m$, used in the calculation of the fatigue limit considering the natural defects of the material, according to Eq. (13). To calculate the fatigue limit considering the presence of the microhole, according to Eq. (12), it was only necessary to calculate its projected area in the direction of the maximum principal stress in tension, according to the definition of the $\sqrt{area}$ parameter. Due to the geometry of the manufactured hole, the area of its projection forms a square with sides equal to the diameter of the hole, therefore, the computed value of $\sqrt{area}$ was $550\ \mu m$.

The results obtained for the fatigue limits from the $\sqrt{area}$ parameter model, considering the material inclusions and the presence of the microhole, are shown in Table 7. It can be observed a reduction of 19 % in the fatigue limit, regarding a material with a microhole.

Table 7. Fatigue limits of AISI 4140 steel from $\sqrt{area}$ parameter.

Defect type	σ_w (MPa)
Non-metallic inclusions ($\sqrt{area}_{max} = 145\ \mu m$)	271
Microhole ($\sqrt{area} = 550\ \mu m$)	220

3.5.2 Uniaxial and multiaxial fatigue results

The proposed multiaxial criterion (SWT_{mod}) generates a fatigue strength curve, which divides the safe region from the failure region, that is, for loads that generate stresses below this curve, failure is not expected and failure is expected for stresses above it. Considering the fatigue limits obtained from the $\sqrt{area}$ parameter model it is expected that model predictions include the effect of small defects on fatigue strength.

The test results are shown in Tables 5 and 6, and Figures 21 and 22 present the comparison between the experimental data and the curves obtained by the proposed model for non-metallic inclusions and superficial microhole of 550 μm, respectively. The

error bands equal to 15% are represented by dashed lines. The full symbols refer to specimens that failed, whereas the empty ones refer to run-outs. There are some symbols that are superimposed, showing stress levels where there were both, failures and run-outs. The data from smooth specimens are depict in Fig. 21, where uniaxial and in-phase loading conditions are plotted in Fig. 21(a) and the out-of-phase loading conditions are plotted in Fig. 21(b).

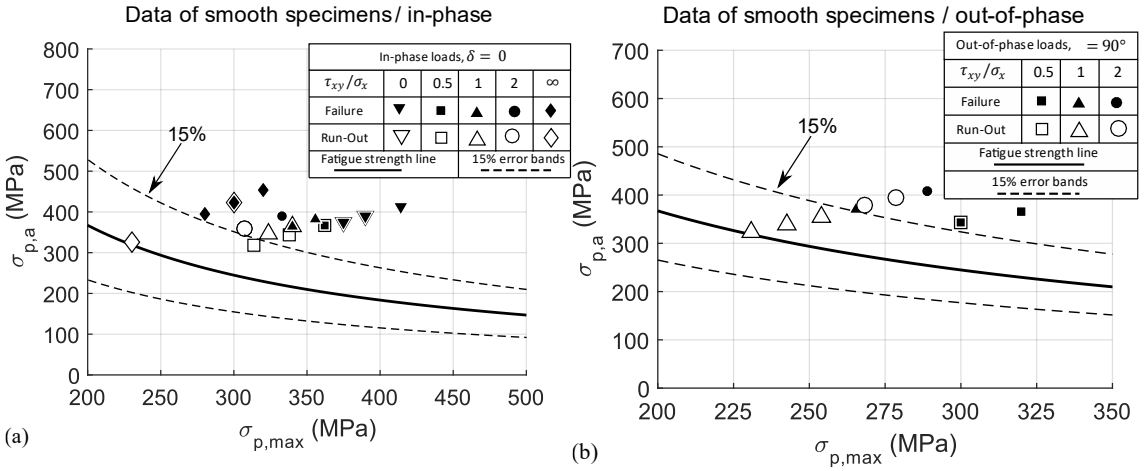

Figure 21. SWT_{mod} prediction and experimental data computed with MRH of smooth specimens, (a) uniaxial and combined in-phase and (b) combined out-of-phase data.

It is remarkable that the forecasts revealed a conservative tendency, especially for the in-phase loads, as shown in Fig. 21(a), where with an error of around 25% the prediction line would coincide with the experimental results and coherently divides the safe region from the danger region. For the combined out-of-phase loads, Fig. 21(b), the predictions are also conservative, but with an error of only 15% the division of the two regions becomes consistent with the experimental results, except for data with a ratio of 2 between the shear stress and the normal stress.

In this case, with smooth specimens, this conservative trend may be associated with the fatigue limit used, which was obtained from a statistical extrapolation of the largest non-metallic inclusion (natural defect) expected to be found in the useful volume of the specimen. However, this inclusion may or may not exist in a specific specimen.

In this scenario, a conservative bias in predicting the fatigue limit is preferable, since the chance of having natural defects of the predicted size is greater in real engineering components, as they have volumes much larger than that of a specimen, as is the case of thermo-generating crankshafts.

In turn, the use of fatigue limits obtained experimentally for naturally defective materials can lead to a non-conservative bias and consequently to fatigue failure. This is due to the limited quantity of specimens and non-homogeneous distribution of natural defects, in which none of the specimens may have critical natural defects that may be present in a real component, much larger than the specimen.

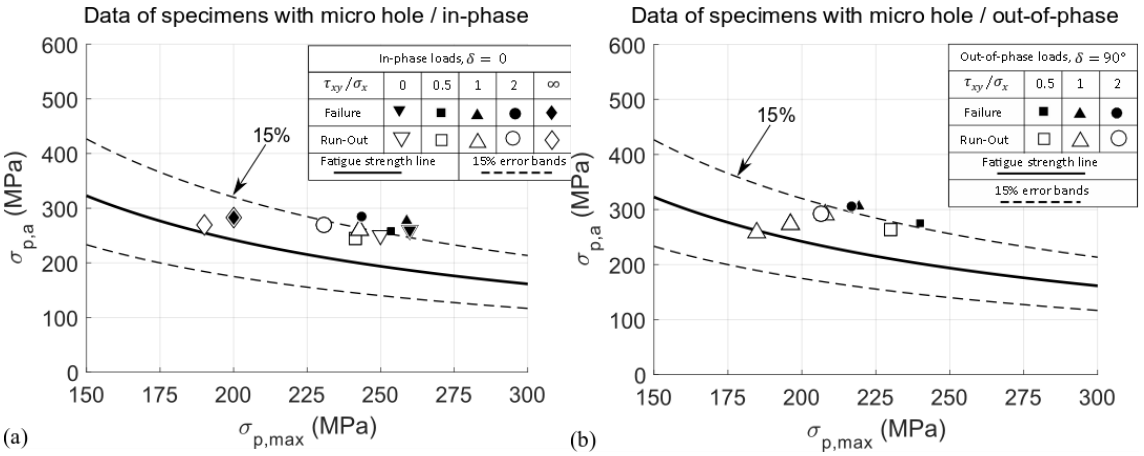

Figure 22. SWT_{mod} prediction and experimental data computed with MRH of specimens with a microhole, (a) uniaxial and combined in-phase and (b) combined out-of-phase data.

Furthermore, in Fig. 22, the experimental data with specimens containing the superficial microhole of 550 µm are shown. Likewise, uniaxial and combined in-phase loading conditions are plotted in Fig. 22(a) and the combined out-of-phase loading conditions are plotted in Fig. 22(b).

For the specimens containing the superficial microhole, the predictions were also conservative in all cases, uniaxial and combined in-phase and out-of-phase loading conditions, with the data around the upper 15% error band. In this case, of specimens with a microhole, we had almost no predictions above the 15%. Additionally, some pure torsion data (Fig. 22 (a)) lied very close to the actual prediction line. This revealed that the model was more accurate in predicting the fatigue strength for large micro superficial defects.

This result is consistent with the comments and observations made earlier. In this case, all specimens tested had the same surface defect size, that is, the same $\sqrt{area}$. In view of this, less dispersion and better predictions in the results were expected.

The fact that the model missed by a range of 15% the large majority of the run-out data for all loading conditions and specimens' configurations tested may be associated

either with the computation of the proposed fatigue parameter, or with the use of the √area parameter to obtain the fatigue limit for this material. Notice that, if the fatigue parameter, which is calculated by means of amplitude and maximum value of principal stresses, somehow overestimates the fatigue damage, the model will indicate failure before it occurs. Also, if the estimated fatigue limit provided by means of the $\sqrt{area}$ parameter is smaller than the actual fatigue limit, the material fatigue strength will be underestimated. Even a combination of both (overestimated fatigue parameter and underestimated fatigue limit) could be the reason for this slightly conservative behavior of the proposed model.

3.5.3 Error Index

The accuracy of the criterion is evaluated through the error index, EI, given by:

$$EI = \frac{R_E - R_P}{R_P} \times 100\% \tag{18}$$

where R_E is the value of the $\mathrm{SWT_{mod}}$ parameter computed for the run-out specimens which lied in the failure region, and R_P is the the value of $\mathrm{SWT_{mod}}$ when it equalizes the fatigue limit. The error index is a way to compare the relative difference between the experimental result (R_E) and the predicted one (R_P). The mean and maximum values of the errors provided by the multiaxial criterion considering the different loading conditions and the specimens conditions are reported in Table 8.

Table 8. Mean and maximum values of the error index.

	Loadings	**Mean** $\boldsymbol{EI}$ %	**Maximum** $\boldsymbol{EI}$ %
Smooth specimen	Uniaxial and combined in-phase	26.41	43.91
	Combined out-of-phase	12.57	22.26
Specimen with a 550 µm microhole	Uniaxial and combined in-phase	11.88	18.18
	Combined out-of-phase	9.86	11.75
All loads		15.18	43.91

As can be observed, the proposed model provided conservative predictions when compared to the experimental data. The lowest value of EI mean, 9.86%, was for the

specimens with a micro hole with combined out-of-phase loading conditions. Even the greatest mean error obtained is around 25%.

This degree of conservatism may be slightly influenced by the stopping criterion established for the tests. Originally, the $\sqrt{area}$ parameter model considers 10^7 cycles as the fatigue limit. However, in this work, the stopping criterion for fatigue tests was defined as 2.10^6, due to operational limitations and reduction in test time.

With this in mind, some tests were performed up to 10^7 cycles on specimens with micro holes and it was found that around 2 million cycles there must be a change in the slope of the SN Curve, known as endurance limit. This is because, among the specimens tested at the same stress level or at very close stresses, those that did not fail before or shortly after the 2 million cycles reached 10^7 cycles without failure, as can be seen in Table 9.

Table 9. Tests conducted until 10^7 cycles with specimens with a 550 μm microhole.

Loading		Cycles
σ_{xa}	260	725,825
	250	10^7 (run-out)
	250	2,596,471
	260	2,677,053
τ_{xya}	200	1,959,328
	190	10^7 (run-out)

Taking this observation into account, we can assume that even if all the tests had been carried out up to 10^7 cycles, there would not be a big change in the results and in the error index, however, this difference would produce smaller errors, increasing the accuracy of the predicted results. Note that, if the tests were extended to 10^7 cycles, some of the tests that reached run-out could fail. Even though such failures were unlikely, if they occurred this would bring the failure points closer to the prediction line of the model.

3.6 Conclusions

In this work, a new multiaxial fatigue model was proposed based on the fatigue limits associated with the $\sqrt{area}$ parameter, according to Murakami. The modified

Smith-Watson and Topper parameter, which is now calculated based on the maximum and amplitude of the principal stresses, proved to be simple to calibrate without the need for fatigue tests. This is because it does not have material constants, and the fatigue limit used is calculated from the $\sqrt{area}$ parameter.

Here it is important to emphasize that the proposed model is capable of predicting only fatigue endurance, aiming for a simple, quick, and cost-effective calibration based on the $\sqrt{area}$ parameter, from which σ_w is obtained. As it involves calculating an equivalent stress, in principle, it would be possible to associate it with S-N curves of the material to obtain an estimate of life. However, this would turn the calibration of the model much more expensive, as the $\sqrt{area}$ parameter looses its validity for finite lives, and then there would be a need to raise specific S-N curves for each artificially defective specimen.

The model was shown to present a slightly conservative behavior, with a mean error of not more than 16% and a maximum error of less than 45%, which was obtained from an outlier whose replica was correctly predicted.

The new multiaxial fatigue model captures well the physical nature of the crack initiation phenomenon. This is because we can now precisely compute the stress amplitude of the principal stress vector. This has an important advantage, as previous research considering naturally defective materials or materials with microdefects has demonstrated that microcracks tend to initiate in or close to planes of maximum principal stresses. Furthermore, the methodology has proven to be of great engineering importance, as it can be applied without the need for S-N curves or long test campaigns to obtain the fatigue limit.

4. ASSESSING FATIGUE IN MATERIALS WITH SMALL DEFECTS: A NEW MULTIAXIAL MODEL BASED ON PRINCIPAL STRESS AMPLITUDES

This chapter is a reproduction of the following publication:

- Araujo LC, Ferreira JL de A, Ziberov M, Araújo JA. Assessing Fatigue in Materials with Small Defects: A New Multiaxial Model Based on Principal Stress Amplitudes. Procedia Structural Integrity 2024;57:144–51

Abstract

A new multiaxial fatigue model for materials containing small defects proposed by the authors is presented, which one can be considered as a modification of the SWT model. This new model relates the fatigue limit of the material obtained from the $\sqrt{area}$ parameter with values associated with the principal stresses. These values are the amplitude of the principal stresses and the maximum principal stress observed. The amplitude value associated with the principal stresses is defined by using the Maximum Variance Method. This amplitude only can be easily obtained under uniaxial loading conditions, but its calculation for torsion, proportional and non-proportional multiaxial loadings is not trivial. Therefore, the calculation of the principal stress amplitude posed a challenge not yet addressed by other authors. The multiaxial fatigue model was evaluated with experimental data from AISI 4140 steel, with several different loading conditions, including uniaxial loading, combined loads in in-phase and out-of-phase configurations. In addition, two types of specimens were used: smooth cylindrical specimens and specimens with a surface micro hole. Comparing the experimental data with the prediction of the new model it was observed that the predictions are slightly conservative with average error not exceeding 6%

.

Keywords: multiaxial fatigue; new model; small defects; principal stress amplitude; maximum variance method.

4.1 Introduction

The investigation of the impact of small defects on the fatigue strength of metallic materials has garnered attention from numerous researchers in recent decades [1,2,16,54]. Notably, the $\sqrt{area}$ parameter proposed by Murakami and Endo [16], along with its adaptations and variations [1,2,40,55], has emerged as a prominent model addressing this issue. Nevertheless, the models based on the $\sqrt{area}$ parameter have predominantly been applied in the context of uniaxial fatigue. In recent years, there has been a surge in studies aimed at exploring the fatigue behavior of materials with small defects under more complex loading conditions [8,11,18–21,28,30,56–58]. This research is crucial due to the prevalence of multiaxial stress states in practical engineering components, arising from either geometric considerations or combined loading scenarios.

This study introduces a novel multiaxial fatigue model proposed by the authors, which can be considered as a modification of Smith, Watson, and Topper (SWT) Criterion [67,68]. This new model establishes a connection between the fatigue limit of the material, determined by the $\sqrt{area}$ parameter, and values associated with the principal stresses induced by the applied loads. These values include their amplitude and the maximum value observed during the loading cycle. Computing these parameters is a non-trivial task, particularly under non-proportional multiaxial loading conditions, where both the magnitude and direction of the principal stresses vary dynamically. Consequently, calculating the amplitude of the principal stresses presented a significant challenge that, to the best of the authors' knowledge, has not yet been addressed by previous researchers.

To evaluate the validity of the proposed model, the authors considered a combination of previously generated and new experimental data of the high strength steel AISI 4140 (DIN 42CrMo4), which is used in the manufacture of various mechanical components. The test data covered a range of loading conditions, such as traction-compression, torsion, and combined loadings with different ratio between shear and normal stresse amplitudes, in-phase and 90° out of phase. In addition, specimens were tested in two conditions: (i) smooth specimens, considering the effect of non-metallic inclusions, and (ii) specimens where a superficial micro hole with a straight bottom was machined with 550 μm in diameter and depth.

4.2 New model proposal

In previous studies on combined loads, it has been observed that small defects can exhibit short, non-propagating cracks in the fatigue limit condition [8,17,39]. These cracks have been found to generally propagate in a direction perpendicular to the maximum principal stress. As a result, several models have been proposed to establish a relationship between the fatigue limit and the values associated with the principal stresses [8,17,66].

In contrast to existing models, which utilize instantaneous values of the principal stresses to calculate fatigue damage, the newly proposed model considers the amplitude value associated with the principal stresses as one of its governing variables. Essentially, this model can be regarded as a modification of the well-known Smith, Watson, and Topper (SWT) Parameter [67,68], and it can be expressed as follows in Eq. 19

$$\mathrm{SWT}_{\mathrm{mod}} = \sqrt{\sigma_{p,max}\sigma_{p,a}} \tag{19}$$

where $\mathrm{SWT}_{\mathrm{mod}}$ represents the Modified Smith, Watson, and Topper parameter, $\sigma_{p,max}$ denotes the maximum value of the greatest principal stress observed at any given time during the loading cycle, and $\sigma_{p,a}$ represents the amplitude of the principal stresses. It is important to note that the calculation of the principal stress amplitude is a complex process, which will be explained in greater detail later on. This relationship offers the advantage of not relying on any material constants. Finally, a mechanical component containing a small defect and subjected to a specific loading history will be deemed safe if the inequality of Eq. 20 is satisfied.

$$\mathrm{SWT}_{\mathrm{mod}} \leq \sigma_w \tag{20}$$

where the equivalent stress, $\mathrm{SWT}_{\mathrm{mod}}$, is obtained from Eq. 19 and σ_w is the uniaxial fatigue strength, which can be easily obtained from the parameter $\sqrt{area}$, as we will see hereafter.

4.2.1 Fatigue Strength Estimation

The model of the parameter $\sqrt{area}$ proposed by Murakami presents a significant advantage in that it enables the estimation of the fatigue strength (σ_w) for materials with micro defects, eliminating the need for actual fatigue tests. When dealing with superficial defects of known size and shape, the model requires the input of the square root of the defect's projected area ($\sqrt{area}$) and the material hardness (Hv) measured in Vickers, as represented by Eq. 21.

$$\sigma_w = \frac{1.43(Hv+120)}{(\sqrt{area})^{1/6}} \tag{21}$$

In the Eq. 21, σ_w represents the fatigue limit in MPa for materials with micro defects, Hv denotes the Vickers hardness measured in kgf/mm^2, and $\sqrt{area}$ is expressed in μm. It should be noted that the plane on which the defect's area is projected is the one perpendicular to the direction of the greatest principal stress under uniaxial loading conditions.

However, when it comes to determining the area of internal defects like non-metallic inclusions or pores, which can exist in varying quantities, sizes, and shapes, a statistical analysis must be conducted to determine the likely largest defect present based on the volume of material. This largest estimated defect is referred to as $\sqrt{area}_{max}$ [2,37,65].

Murakami considered the most detrimental type of internal defect to be the one in direct contact with the free surface. When a crack originates around this type of defect, it typically propagates and occupies the entire weakened area between the defect and the free surface. This "extra" area must be taken into account when calculating the $\sqrt{area}$. Consequently, the lower bound of the uniaxial fatigue limit is defined as follows:

$$\sigma_w = \frac{1.41(Hv+120)}{(\sqrt{area}_{max})^{1/6}} \tag{22}$$

4.2.2 Principal stresses amplitude

A mechanical component under a loading history, such as the following described by Eqs. 23 and 24, that includes normal stress amplitude (σ_{xa}) and shear stress amplitude (τ_{xya}), along with angular frequency (ω), time (t), and phase angle (δ).

$$\sigma_x = \sigma_{xa} \sin \omega t \tag{23}$$

$$\tau_{xy} = \tau_{xya} \sin(\omega t + \delta) \tag{24}$$

For each instant of time, the maximum and minimum principal stresses and their corresponding directions can be obtained using eigenvalues and eigenvectors of the stress tensor generated [68]. With a cyclic loading history, each principal stress vector, $\boldsymbol{\sigma_{p,max}}$ and $\boldsymbol{\sigma_{p,min}}$, traces a closed path, for example, see Fig. 23, where the path described by the principal stresses for a combined and out-of-phase loading are depicted. By applying the Maximum Variance Method (MVM) [75] in the history of the principal stresses, the amplitude of the principal stresses, $\sigma_{p,a}$, can be computed.

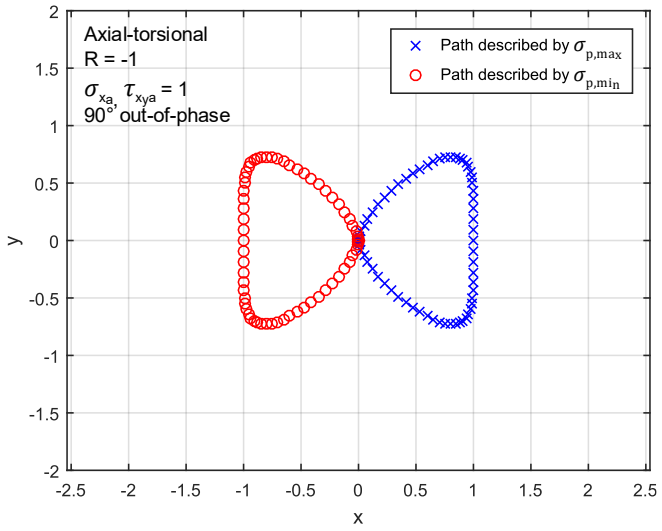

Figure 23. Path described by the principal stresses in combined out-of-phase loading.

The variance, a statistical measure, plays a crucial role in assessing the dispersion of events within a random process relative to their mean value. Several studies conducted by researchers have demonstrated that the fatigue damage is significantly influenced by the variance of the stress history [75]. In this work the measure of the variance of the set of the two principal stresses, maximum and minimum, which will be

called $\boldsymbol{\sigma_p}$, is used to obtain the so-called amplitude of principal stresses, $\sigma_{p,a}$, one of the determining values for the calculation of the fatigue parameter. In the following is shown the proposed methodology for calculating $\sigma_{p,a}$, using the Maximum Variance Method. Considering the principal stresses histories σ_p(t), that can be decomposed in σ_{px}(t) and σ_{py}(t) that will be restricted to the reference plane (x,y) in plane stress state, we can define the covariance matrix expressed by Eq. 25.

$$u_\Delta = \begin{bmatrix} u_{\sigma_{px}} & u_{\sigma_{px},\sigma_{py}} \\ u_{\sigma_{px},\sigma_{py}} & u_{\sigma_{py}} \end{bmatrix} = \begin{bmatrix} Var[\sigma_{px}(t)] & Cov[\sigma_{px}(t),\sigma_{py}(t)] \\ Cov[\sigma_{px}(t),\sigma_{py}(t)] & Var[\sigma_{py}(t)] \end{bmatrix} \quad (25)$$

In Eq. 25, $Var[\,]$ represents the statistic calculation of the variance of the elements between the brackets and $Cov[\,]$ the calculation of the covariance of the elements between the brackets.

The eigenvalues of u_Δ define the maximum variance and can be obtained with Eq. 26, the eigenvectors define the orientation of the maximum variance in the analyzed plane. Finally, the equivalent value of the principal stresses amplitude can be obtained with Eq. 27. A detailed explanation of the MVM used can be found in the work of Ferreira [75].

$$\lambda_{1,2} = \frac{u_{\Delta 11}+u_{\Delta 22}}{2} \pm \sqrt{\left(\frac{u_{\Delta 11}+u_{\Delta 22}}{2}\right)^2 + (u_{\Delta 12})^2} \quad (26)$$

$$\sigma_{p,a} = \sqrt{2(\lambda_1+\lambda_2)} \quad (27)$$

4.3 Experimental campaign

4.3.1 Material and specimens

The experimental campaign was conducted with fatigue specimens made of AISI 4140 (42CrMo4) steel, oil quenched, and tempered around 600 °C. The material was removed from crankshafts of stationary generators that failed due to fatigue during operation. Table 10 provides the mechanical properties of the AISI 4140 steel, which were determined through a single tensile test conducted at a displacement rate of

0.5mm/min. The Vickers hardness was measured by averaging ten readings from three different samples, with a load of 100 kgf.

The specimens used in the experiment were designed following ASTM E466-15 standards and had a circular cross-section, with 10 mm in diameter. Two types of cylindrical specimens were utilized: (i) smooth specimens without artificially introduced surface defects, and (ii) specimens containing a machined micro surface hole with a diameter and depth of 550 μm.

Table 10. Mechanical properties of AISI 4140 steel.

Young's modulus (GPa)	0.2%-offset yield stress (MPa)	Tensile strength (MPa)	Elongation (%)	Vickers hardness (kgf/mm2)
202	647	932	20	320

4.3.2 Fatigue tests

Fatigue tests were performed under force control in accordance with ASTM E466-15 in an axial (100 kN capacity) and an axial-torsional (100 kN e 1100 Nm) servo-hydraulic testing machines. The tests were conducted in room temperature and the frequencies kept between 5 and 15 Hz, depending on the load level. All tests were carried out with totally alternating sine waves, that is, with a loading ratio R of -1.

Fatigue tests were conducted to examine various ratios between shear stress amplitudes (τ_{xya}) and normal stress amplitudes (σ_{xa}). The ratios considered were 0, 0.5, 1, 2, and ∞, representing traction-compression, combined loads, and pure torsion. Both in-phase and 90º out-of-phase tests were performed for the combined loads.

The objective of these tests was to observe at least one failure and one run-out for each type of loading condition. A run-out was defined as the point where the specimen did not fail within a specified number of cycles, which was set at 2.10^6 cycles. A complete rupture of the specimen was used as the failure criterion. If a specimen failed, the stress level was reduced for the subsequent test. Conversely, if the run-out was reached, the next test would be performed at an incrementally higher stress level using a new specimen. In other words, no specimen was reused during the evaluation of the proposed multiaxial model.

4.4 Results and discussion

4.4.1 Fatigue strength from $\sqrt{area}$ parameter

In the work of Machado [11], were conducted an analysis of inclusions and used the extreme statistics method to compute the value o$\sqrt{area_{max}}$ of 145 μm. This value was used in the calculation of the fatigue limit, taking into account the natural defects of the material, as per Eq. 22. For the calculation of the fatigue limit considering the presence of the micro hole, as per Eq. 21, it was only necessary to calculate the projected area of the hole in the direction of the maximum principal stress in tension. Due to the geometry of the manufactured hole, the projected area forms a square with sides equal to the diameter of the hole, resulting in a computed value of $\sqrt{area}$ of 550 μm. The results obtained for the fatigue strength using the $\sqrt{area}$ parameter model, considering the material inclusions and the presence of the micro-hole, are presented in Tab. 11.

Table 11. Fatigue strengths of AISI 4140 steel from $\sqrt{area}$ parameter model.

Defect	Fatigue strength (MPa)
Non-metallic inclusions	271
Micro-hole	220

4.4.2 Fatigue data and predictions of the proposed model (SWTmod)

The proposed multiaxial criterion (SWT_{mod}) generates a fatigue strength curve that separates the safe region from the failure region. Stresses below this curve are expected to result in run-outs, while stresses above it indicate potential failure. By considering the fatigue limits obtained from the $\sqrt{area}$ parameter model, the proposed model is expected to account for the influence of small defects on fatigue strength.

Figures 24 and 25 illustrate the comparison between experimental data points and the curves obtained with the proposed model for the fatigue strength for non-metallic inclusions and superficial micro holes, respectively. Dashed lines represent error bands of 15%. Full symbols represent specimens that failed, while empty symbols represent run-outs. Some symbols may overlap, indicating stress levels where both failures and run-

outs occurred. Fig. 24 specifically depicts data from smooth specimens, with Fig. 24(a) showing in-phase loading conditions and Fig. 24(b) presenting out-of-phase loading conditions.

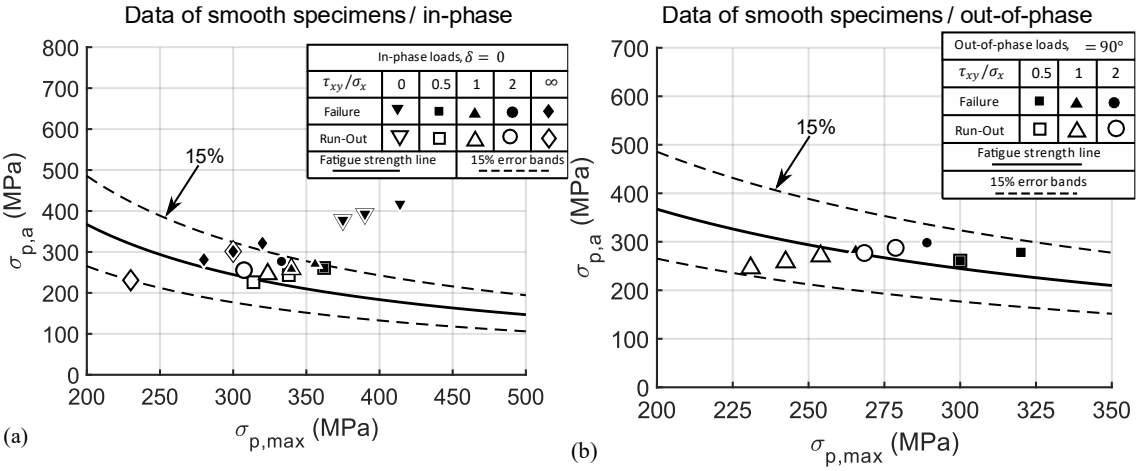

Figure 24. SWT_{mod} prediction and experimental data of smooth specimens, (a) uniaxial and combined in-phase and (b) combined out-of-phase data.

Additionally, Fig. 25 presents the experimental data obtained from specimens containing the superficial micro hole. Fig. 25(a) displays the results for uniaxial and combined in-phase loading conditions, while Fig. 25(b) represents the combined out-of-phase loading conditions.

Remarkably, the predictions turned out to be very accurate, with the vast majority of points within the 15% error bands. There was a slightly conservative trend for the smooth specimens, with some run-outs in the fault region, Fig. 24(a), and a slightly non-conservative trend for the micro-hole specimens, with some faults in the region where run-outs were expected, Fig. 25(a). Except for the uniaxial tensile-compression test data for smooth specimens, all points were within or very close to the 15% error bands.

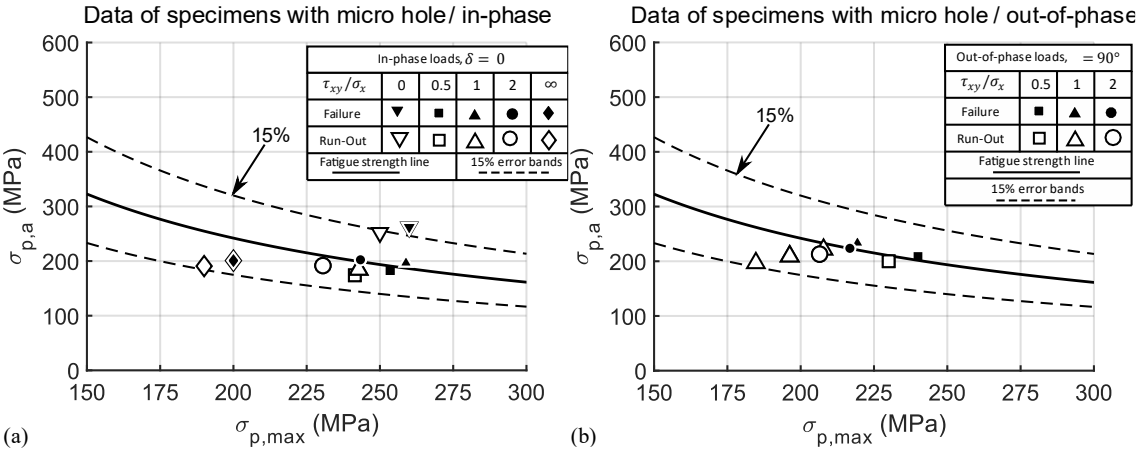

Figure 25. SWT_{mod} prediction and experimental data of specimens with a micro hole, (a) uniaxial and combined in-phase and (b) combined out-of-phase data.

The accuracy of the criterion was also assessed using the error index (EI) in Eq. 28, which quantifies the relative difference between the experimental result (R_E) and the predicted result (R_P). The average and maximum values of the errors obtained from the multiaxial criterion, considering various loading conditions and specimen conditions, are presented in Tab. 12.

$$EI = \frac{R_E - R_P}{R_P} \times 100\% \tag{28}$$

Table 12. Fatigue strengths of AISI 4140 steel from $\sqrt{area}$ parameter model.

	Loadings	Mean EI %	Maximum EI %
Smooth specimen	Uniaxial and combined in-phase	14.87	44.48
	Combined out-of-phase	2.75	4.45
Specimen with micro hole	Uniaxial and combined in-phase	3.88	18.65
	Combined out-of-phase	0	0
All loads		5.38	44.48

4.5 Conclusions

In this study, a novel multiaxial fatigue model based on the $\sqrt{area}$ parameter was introduced. The modified Smith-Watson and Topper parameter, incorporating the maximum principal stress and the amplitude of the principal stresses obtained using the

Maximum Variance Method, was found to be easy to calibrate without the need for fatigue testing, as it does not rely on material constants. The fatigue limit used in the model was calculated based on the $\sqrt{area}$parameter, eliminating the need for additional tests.

The proposed model was evaluated using experimental data from a high-strength steel known to be sensitive to small defects. The specimens were tested under two conditions: smooth, without artificially introduced defects, and with a superficial micro hole. Different loading conditions were applied during testing.

The accuracy of the model's predictions was assessed using an error index compared to the experimental data. The model demonstrated high accuracy, with a mean error below 6% and a maximum error below 45%. Larger errors exceeding 15% were only observed for one specific loading condition among the various conditions tested.

Overall, the new multiaxial fatigue model yielded satisfactory results when compared to the data obtained from AISI 4140 steel under various loading conditions, considering both the estimated maximum non-metallic inclusion and the superficial micro hole present in the specimens.

5. NEW TESTS AND MULTIAXIAL FATIGUE MODELLING OF STEELS WITH DIFFERENT SMALL DEFECTS

This chapter is a reproduction of a work that is in the process of publication. It presents new fatigue data for AISI 4140 steel, focusing on specimens with a microhole of 350 μm in diameter and depth, subjected to various loading conditions. Additionally, new fatigue data for AISI 4340 steel are provided, also subjected to various loading conditions, considering two scenarios: specimens with only the natural defects of the material and those with a surface microhole of 350 μm in diameter and depth. These new datasets will be used to further evaluate the performance and applicability of the novel multiaxial fatigue model introduced in Chapters 3 and 4, assessing its range and predictive capability.

Abstract

A new multiaxial fatigue model for metallic materials containing small defects (SWTmod) was recently presented by the authors [35,36]. This model correlates the uniaxial fatigue limit derived from the √area parameter [2] of high-strength steel containing small defects with the maximum principal stress and the amplitude of the principal stresses, whose calculation under non-proportional loading is non-trivial. In this work, the model's performance is further evaluated with new multiaxial fatigue data from AISI 4140 and 4340 steels under various loading conditions, including specimens with only their natural defects and specimens with a superficial microhole. The proposed model provided satisfactory fatigue strength estimates, with a simple, fast, and cost-effective calibration process, which is of great interest for engineering calculation purposes.

keywords: Multiaxial fatigue; Small defects; √area Parameter; Principal stresses amplitude.

5.1 Introduction

The impact of small defects and non-metallic inclusions on fatigue strength has been widely studied over the years [2,8]. The presence of these imperfections intensifies stress concentration, accelerating fatigue crack initiation and reducing the component's working life [9,10]. The fatigue strength of high-strength steels is considerably affected by the presence of microscopic defects. This effect has been evidenced in real-world failures, such as the recent cases of crankshaft fractures in Brazilian thermoelectric power plants (Fig. 26). After investigation, it was determined that the cause of these failures was the presence of numerous non-metallic inclusions in the material. These crankshafts, made of AISI 4140 (DIN 42CrMo4) or AISI 4340 (DIN 34CrNiMo6) steel, suffered premature fatigue damage due to these impurities. This type of failure can cause major disruption in industry and extremely high financial losses.

Crankshafts are subjected to cyclic loading conditions due to radial forces generated by combustion pressure, transmitted by pistons and connecting rods. This leads to harmonic torsion combined with cyclic bending, creating conditions for fatigue damage over time. Ideally, these components are designed for infinite life, enduring millions of loading cycles. However, inadequate consideration or complete disregard of small defects in the design process can lead to incorrect material specifications and fatigue failures, as cracks tend to initiate in these regions, as in the case mentioned above [11]

In fact, numerous studies report fatigue failures caused by small defects and non-metallic inclusions in critical engineering components, including wind turbine gearboxes, railway wheels, pipelines, turbine blades, and crankshafts [12–15]. Many of these components are subjected to time-varying multiaxial stresses throughout their operational life. Despite extensive research on fatigue in materials with small defects, most studies have been conducted under uniaxial loading conditions. Investigations into multiaxial fatigue behavior in the presence of small defects remain scarce, though interest in this area has grown significantly in recent years. Given the prevalence of real-world failures and the complex stress states experienced by critical components, the study of multiaxial fatigue in defective materials is an increasingly relevant and urgent topic.

a

b

Figure 26. (a) crankshaft of a thermoelectric generator that failed in a Brazilian power plant, (b) fatigue crack in the crankshaft.

This work presents new fatigue data for AISI 4140 steel, focusing on specimens with a microhole of 350 μm in diameter and depth, subjected to various loading conditions. Additionally, new fatigue data for AISI 4340 steel are provided, also subjected to various loading conditions, considering two scenarios: specimens with only the natural defects of the material and those with a surface microhole of 350 μm in diameter and depth. These new datasets will be used to further evaluate the performance and applicability of the novel multiaxial fatigue model introduced in by the author in [35,36], assessing its range and predictive capability.

This work also compares the results obtained with the Maximum Rectangular Hull (MRH) [69] and the Maximum Variance Method (MVM) [75], used in the calculation of the amplitude of the principal stresses, for fatigue strength predictions with the new proposed model. At the end, a comparative table is presented with the results of the average errors of the predictions, with different methods of calculating the amplitude, in order to evaluate the most efficient one.

5.2 Multiaxial Model Proposal

As mentioned by Araujo *et. al* in [35], experimental studies involving combined loading conditions have consistently shown that, under fatigue limit scenarios, short non-propagating cracks tend to initiate from small defects such as inclusions or voids [8,17,39]. These cracks generally develop in directions nearly perpendicular to the axis of the maximum principal stress. Based on these observations, some models have been proposed that correlate the fatigue limit with parameters related to principal stress values [8,17,66].

In view of this, a new multiaxial fatigue endurance model was developed by the authors [35]. The new model introduces the amplitude of the principal stresses associated with the maximum principal stress as key variables in its formulation. In essence, as mentioned in the previous works, this new model can be considered as a modification of the Smith, Watson, and Topper (SWT) parameter [67,68], and is defined as:

$$\mathrm{SWT}_{\mathrm{mod}} = \sqrt{\sigma_{p,max}\sigma_{p,a}} \tag{29}$$

where $\mathrm{SWT}_{\mathrm{mod}}$ represents the modified SWT parameter, $\sigma_{p,max}$ is the the maximum value of the principal stress during a full loading cycle and $\sigma_{p,a}$ is the amplitude of the principal stresses.

One of the main advantages of this formulation is that it does not require any material-dependent constants, enhancing its applicability. A mechanical component containing a small defect can be considered safe under multiaxial cyclic loading if the following criterion is satisfied:

$$\mathrm{SWT}_{\mathrm{mod}} \leq \sigma_w \tag{30}$$

where the fatigue parameter, $\mathrm{SWT}_{\mathrm{mod}}$, is obtained from Eq. (29) and the uniaxial fatigue limit, σ_w, can be obtained from the $\sqrt{area}$ parameter, as will be presented further down.

5.2.1 Determining the Principal Stresses Amplitude

Considering a typical loading scenario composed of time-varying axial and torsional components, at each instant in time, the maximum and minimum principal stresses and their respective directions can be determined by computing the eigenvalues and eigenvectors of the Cauchy stress tensor [68].

Over a full cycle, the principal stress vector traces out a closed path in the stress space. There are several mathematical methods used to calculate the mean value and the amplitude of a vector that varies in time, such as the Minimum Circumscribed Circumference (MCC) [50,76], the Minimum Ellipse Method [77], the Moment of Inertia Method [78,79], the Maximum Rectangular Hull (MRH) [69,80] and the Maximum Variance Method (MVM) [75], among others [44,81,82]. All these methods can be applied to quantify the amplitude of the principal streses, $\sigma_{p,a}$, although this work will mainly consider the Maximum Rectangular Hull (MRH) and the Maximum Variance Method (MVM). The use of these methods is particularly useful because they accommodate complex, non-proportional loading histories, including cases where all three principal stresses vary over time.

The MRH defines stress amplitude as half the length of the diagonal of the smallest rectangle that fully encloses the path of the principal stress vector in the space. With a cyclic loading history, each principal stress component, $\boldsymbol{\sigma_1}$, $\boldsymbol{\sigma_2}$ and/or $\boldsymbol{\sigma_3}$, will describe a closed path. By plotting the paths described by the principal stress vector components and applying the Maximum Rectangular Hull method (MRH) it is possible to compute the amplitude of the principal stresses, $\sigma_{p,a}$. A major advantage of the MRH is that it is simple to implement, and it can consider the effect of non-proportional stress histories. More details about the implementation of MRH method can be found in refs. [69,80] and about the application of the MRH in the $\mathrm{SWT_{mod}}$ criteria, see ref. [35].

Throughout the studies, it was observed that using the Maximum Rectangular Hull method (MRH) to calculate the amplitude of the principal stresses may not be the best alternative for this purpose [36]. Another method that has been tested as a possible alternative for calculating the amplitude of the principal stresses is the Maximum Variance Method [75], by applying this method in the history of the principal stress vector, the amplitude of the principal stresses, $\sigma_{p,a}$, can be computed. The variance, a statistical measure, plays a crucial role in assessing the dispersion of events within a

random process relative to their mean value. Several studies conducted by researchers have demonstrated that the fatigue damage is significantly influenced by the variance of the stress history. More details about the implementation of this method can be found in [36,75].

5.2.2 Fatigue Limit Estimation Using the $\sqrt{area}$ Parameter

The fatigue limit used in the proposed SWT_{mod} model can be either experimentally determined for each material or estimated through analytical approaches. For defect-free materials, or when the influence of micro-defects is negligible, using experimentally obtained fatigue limits often yields reliable results. However, when small defects are present, as is frequently the case in industrial materials, the use of the $\sqrt{area}$ parameter to estimate the fatigue limit proves to be substantially more advantageous. This approach not only drastically reduces the time and cost associated with extensive fatigue testing but also tends to yield more conservative and reliable fatigue limits. In contrast, experimental fatigue limits for materials with small defects may lead to underestimated results due to the inherent complexity and variability of defect-related crack initiation [11,28,30].

The model based on the $\sqrt{area}$ parameter, originally proposed by Murakami and Endo, offers a practical and effective means of estimating the fatigue strength (σ_w) of materials containing micro-defects, without the need for costly and time-consuming fatigue testing [1,2,16]. When the size and shape of surface defects are known, the model requires only the material's Vickers hardness (Hv) and the square root of the projected area of the defect ($\sqrt{area}$), which can be easily calculated. The relationship is expressed as follows:

$$\sigma_w = \frac{1.43(Hv+120)}{(\sqrt{area})^{1/6}} \tag{31}$$

In Eq. (31), σ_w represents the fatigue limit in MPa, Hv is the Vickers hardness in kgf/mm², and $\sqrt{area}$ is given in micrometers (μm). The defect area should be projected onto the plane perpendicular to the direction of the maximum principal stress under uniaxial loading conditions.

For internal defects such as non-metallic inclusions or pores, which vary in shape, size, and spatial distribution, a statistical approach is required to estimate the most critical defect likely to occur within a given volume of material. The largest statistically expected defect is referred to as $\sqrt{area}_{max}$, and is used in a modified form of the equation to ensure a conservative estimation of fatigue strength. For more details of the statistical analysis see refs [2,37,40,41].

Murakami identified the most detrimental type of defect as one located in direct contact with the material's free surface. In such cases, crack initiation typically occurs at the interface between the defect and the surface, and the crack rapidly propagates through the weakened zone. The total effective crack area must therefore include this additional surface-influenced region. As a result, the lower-bound estimation of the fatigue limit is given by:

$$\sigma_w = \frac{1.41(Hv+120)}{(\sqrt{area}_{max})^{1/6}} \tag{32}$$

This formulation is particularly useful for high-strength steels and other structural alloys where microstructural inclusions are often unavoidable, and where reliable fatigue design must account for their influence.

5.3 Experimental Program

5.3.1 Material and specimens

The materials investigated in this study were AISI 4140 (42CrMo4) steel and AISI 4340 (34CrNiMo6). The materials were removed from the crankshafts of stationary generators that failed due to fatigue during operation. Table 13 lists the chemical composition of the materials, which was obtained by optical emission analysis according to ASTM standard A751. Although the properties of AISI 4140 have been previously described in the literature, see refs [6,35], they will be thoroughly detailed here for the sake of completeness.

The microstructure of the 4140 steel is shown in Fig. 27, and Fig. 28 shows the microstructure of 4340, where, for both materials, the transverse and longitudinal sections

were defined relative to the longitudinal axis of the specimen (refer to Fig. 29). The metallographic samples were polished and etched with 5% nitric acid solution in ethanol and examined using optical microscopy. In the 4140 steel (Fig. 27) it is possible to identify in the microstructure regions with thick phases of light tone that correspond to α-ferrite; it can also be observed elongated regions with α-ferrite and cementite (Fe3C) phases, which are characteristic of tempered martensite. In the 4340 steel (Fig. 28), only tempered martensite characteristics are observed. The non-metallic inclusions were analyzed by Energy Dispersive X-ray Spectroscopy, which revealed that their chemical composition was mainly composed of aluminum (Al), silicon (Si), and oxygen (O).

Table 13. Chemical composition of AISI 4140 and 4340 (wt. %).

	C	Si	Mn	Ni	Cr	Mo	Fe
4140	0.41	0.08	0.82	0.80	1.01	0.25	Balance
4340	0.35	0.26	0.49	1.57	1.44	0.29	Balance

Table 14 lists the measured mechanical properties of the materials in standard tensile tests. The Vickers hardness was measured using an applied load of 100 kgf.

The geometry of the solid cylindrical specimens used in the fatigue tests is shown in Fig. 29. The specimen manufacturing process consisted of cutting the material into prisms, followed by machining to the final geometry and polishing to achieve a roughness less than 0.2 μm. These specimens were designed according to ASTM E466-15.

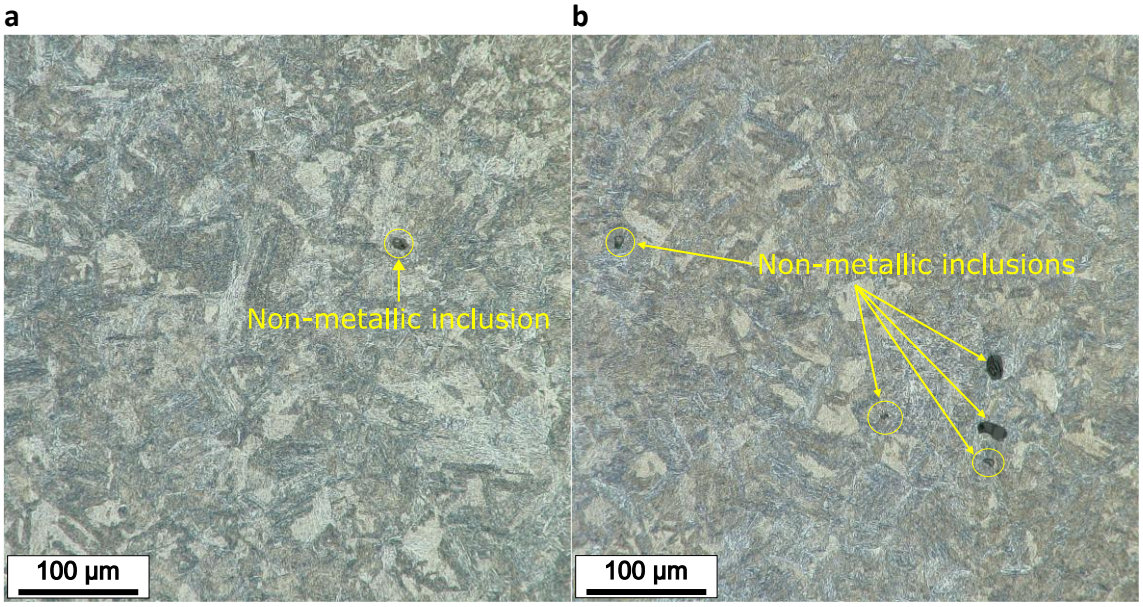

Figure 27. Microstructure of 4140 steel: (a) transverse section and (b) longitudinal section of the solid cylindrical specimen [6].

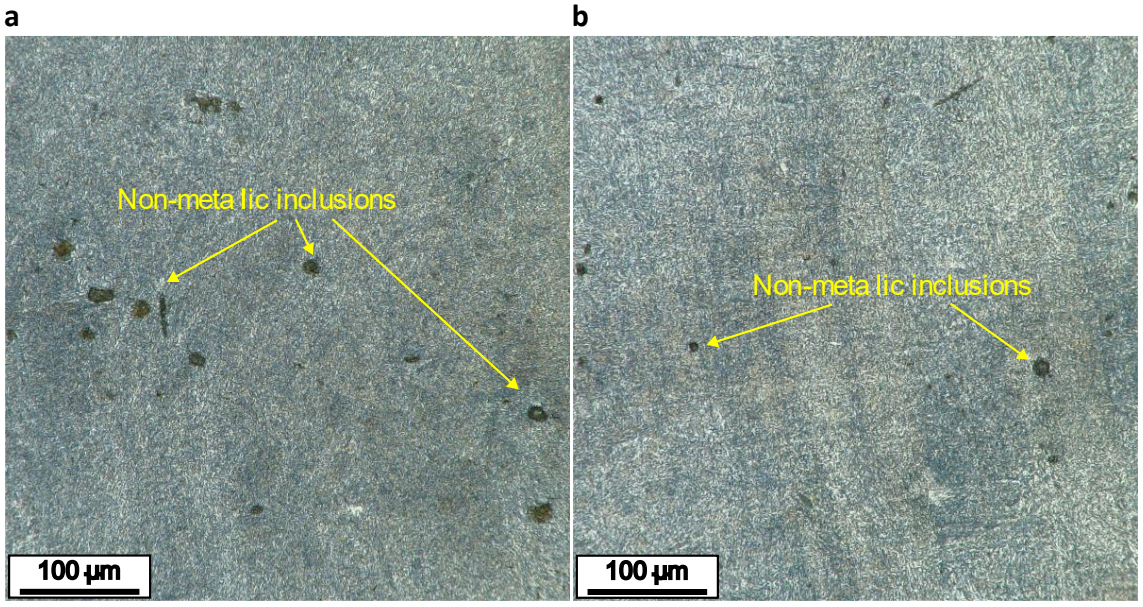

Figure 28. Microstructure of 4340 steel: (a) transverse section and (b) longitudinal section of the solid cylindrical specimen.

Table 14. Mechanical properties of the materials.

	Young's modulus (GPa)	0.2%-offset yield stress (MPa)	Ultimate tensile strength (MPa)	Elongation (%)	Vickers hardness (kgf/mm2)
4140	202	647	932	20	320
4340	207	760	900	20	300

The investigation involved specimens in two different conditions: (i) plain specimens without any visible surface defect; and (ii) specimens with a cylindrical blind microhole, which was artificially introduced into the specimen surface. In each specimen, a single microhole was machined, with a diameter (Ø) and depth (h) of 350 μm, see Fig. 29. The purpose of these microholes was to simulate surface defects much larger than the inclusions of the material, which may originate in a component by external action. Although they exist, residual stresses due to the machining process were disregarded in the analyses carried out.

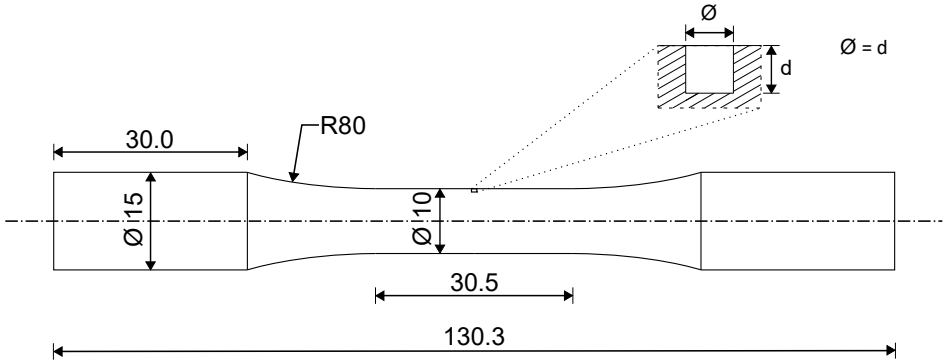

Figure 29. Specimen used in the fatigue tests (dimensions in mm) and detail in the case of specimens with cylindrical microhole [6].

As in the previous works, the machining of the microholes were performed in a CNC XH7132, with 3 axis and positioning resolution of 15 μm. To achieve the straight bottom, helical hole milling was used. This process is also preferable because it lowers cutting forces and produces higher surface quality than mechanical drilling [70]. In this sense, the selected tool was a WC micro end mill coated with TiAlN with 300 μm diameter. The cutting parameters were selected based on the literature [71,72] and improved in preliminary micro milling trials, resulting in a cutting velocity of 9,4 m/min, feed per tooth of 3,3 μm and a depth setting of the helical course of 25 μm.

During the micro milling procedure, cutting fluid was used to achieve a better finish on the microhole surfaces. Considering that the literature reports that dry micro milling or insufficient cutting fluid can lead to lower quality, higher surface roughness values, and adherence of material burr formation [73] synthetic cutting fluid Bio100e was diluted in water in a 1:9 ratio and applied at a flow rate of 6.0 l/min to ensure that the cut occurred submerged or in a near-submerged method, which increased the integrity of the specimens [74].

5.3.2 Fatigue tests

As in previous studies, the tests were conducted under force control using MTS servo-hydraulic testing machines. A complete set of new tests were produced with a material that was not considered before, the 4340 steel, which is a naturally defective material. The tests were performed under fully reversed loading and were characterized by the ratio τ_{xya}/σ_{xa} between the shear and axial stress amplitudes. The tension-compression and torsion tests have ratio 0 and ∞, respectively.

For the newly studied material, 4340 steel, tests were performed only in smooth specimens in uniaxial tension-compression, torsion and various combined loading conditions, with applied load ratios (τ_{xya}/σ_{xa}) of 0, 0.5, 1, 2, and ∞. This testing strategy was specifically designed to assess the influence of natural defects in the material, particularly non-metallic inclusions, on its fatigue behavior under different multiaxial stress states.

New tests on 4140 steel were performed on specimens containing a microhole of 350 μm in diameter and depth, also with various ratios between shear stress amplitude (τ_{xya}) and normal stress amplitude (σ_{xa}), specifically 0, 0.5, 1, 2, and ∞. For the ratio equal 1, tests were carried out both, in-phase and 45° out-of-phase.

The primary objective of all tests was to obtain at least one failure and one run-out for each different loading condition. In these tests, a run-out was defined as reaching 2×10^6 cycles without failure, while complete specimen fracture served as the criterion for failure.

The following tables show the data obtained for each test carried out on the two materials. Table 15 presents the results for the 4140 steel from uniaxial and combined in-

phase tests, as well as the data from the 45° out-of-phase tests. Table 16 lists the data for 4340 steel specimens without a microhole and specimens with a 350 μm microhole.

Table 15. 4140 steel test data of specimens with a 350 μm micro hole.

	Test	σ_{xa}	τ_{xya}	$\frac{\tau_{xya}}{\sigma_{xa}}$	Cycles
Uniaxial and combined in-phase	1	260	0	0	run-out
	2	280	0	0	run-out
	3	300	0	0	run-out
	4	320	0	0	1764542
	5	320	0	0	1548071
	6	250	125	0.5	run-out
	7	270	135	0.5	359417
	8	260	130	0.5	347946
	9	250	125	0.5	490654
	10	230	115	0.5	1292140
	11	190	190	1	1269072
	12	200	200	1	607080
	13	180	180	1	run-out
	14	190	190	1	1135077
	15	100	200	2	run-out
	16	110	220	2	run-out
	17	120	240	2	741228
	18	120	240	2	720543
	19	0	280	inf	1370678
	20	0	280	inf	1937435
	21	0	260	inf	run-out
Combined 45° out-of-phase	1	200	200	1	320968
	2	190	190	1	754569
	3	180	180	1	run-out
	4	180	180	1	701233
	5	180	180	1	1626274
	6	190	190	1	989489

Table 16. 4340 steel test data.

	Test	σ_{xa}	τ_{xya}	$\frac{\tau_{xya}}{\sigma_{xa}}$	Cycles
Smooth specimens	1	390	0	0	1127337
	2	390	0	0	263798
	3	390	0	0	run-out
	4	410	0	0	run-out
	5	410	0	0	467218
	6	410	0	0	618985
	7	430	0	0	run-out
	8	430	0	0	run-out
	9	430	0	0	277181
	10	430	0	0	348160
	11	430	0	0	274389
	12	320	160	0.5	1122637
	13	320	160	0.5	run-out
	14	340	170	0.5	run-out
	15	340	170	0.5	289772
	16	340	170	0.5	153259
	17	220	220	1	run-out
	18	230	230	1	run-out
	19	240	240	1	590137
	20	240	240	1	538048
	21	230	230	1	run-out
	22	140	280	2	249196
	23	130	260	2	1853910
	24	130	260	2	run-out
	25	140	280	2	655386
	26	0	280	inf	run-out
	27	0	300	inf	1418391
	28	0	300	Inf	run-out
	29	0	320	inf	276275
	30	0	320	inf	299266
	31	0	280	inf	run-out
	32	0	280	inf	551394
	33	0	290	inf	run-out
	34	0	290	inf	run-out

5.4 Results and discussion

5.4.1 Fatigue limits from $\sqrt{area}$ parameter

In the same way as reported in [11], for 4140 steel, the analysis of the inclusion content of 4340 steel was also carried out to estimate the $\sqrt{area}_{max}$ using the Extreme Statistics Method and to calculate the fatigue limit for natural defects [37,41,65]. From the analysis on a sample cut 90° relative to the longitudinal axis of the specimen, the area of 60 inclusions was measured in standard inspection areas, giving the $\sqrt{area}_{\max}$ distribution shown in Fig. 30.

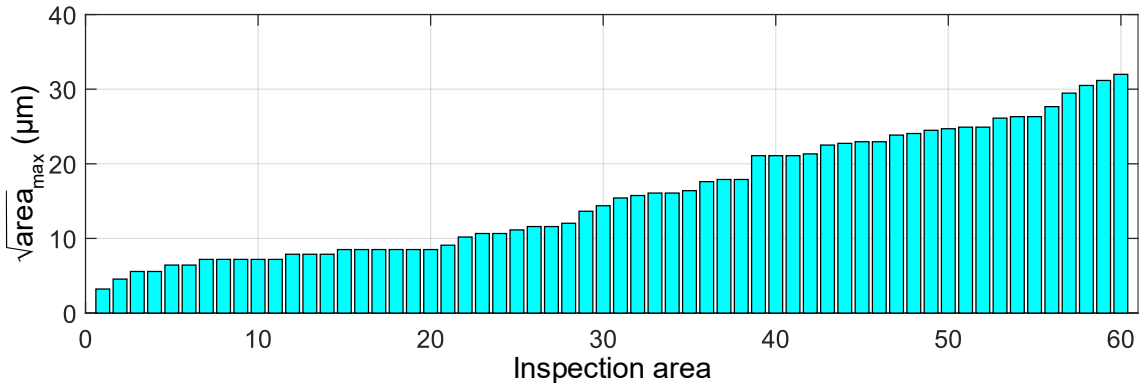

Figure 30. Square root of the projected area of the inclusion of maximum size in ascending order, for the inspection areas of the 4340 steel sample cut at 90°.

From the inclusions analysis and the extreme statistics method, conducted in the 4340 steel, the computed value of $\sqrt{area}_{max}$ was 95 μm, this value is used in the calculation of the fatigue limit considering the natural defects of the material, according to Eq. (32). To calculate the fatigue limit considering the presence of the microhole, according to Eq. (31), it was only necessary to calculate its projected area in the direction of the maximum principal stress in tension, according to the definition of the $\sqrt{area}$ parameter. Due to the geometry of the manufactured hole, in the 4140 steel specimens, the area of its projection forms a square with sides equal to the diameter of the hole, therefore, the computed value of $\sqrt{area}$ was 350 μm.

The results obtained for the fatigue limits from the $\sqrt{area}$ parameter model, considering the inclusions in the 4340 steel, and the presence of the microhole in 4140

steel, are shown in Table 17. It is important to cite the Vickers hardness (HV) of the materials, used in $\sqrt{area}$ parameter model: 4140 steel has a HV of 320 kgf/mm^2, while 4340 steel has 300 kgf/mm^2.

Table 17. Fatigue limits of AISI 4140 and 4340 steel from $\sqrt{area}$ parameter.

Material	Defect type	σ_w (MPa)
4140	Microhole ($\sqrt{area} = 350\ \mu m$)	237
4340	Non-metallic inclusions ($\sqrt{area}_{max} = 95\ \mu m$)	277

5.4.2 Comparison between fatigue data and the prediction of the SWT_{mod}

Figures 31 and 32 illustrate the comparison between experimental data points and the curves obtained with the proposed model for the fatigue strength of non-metallic inclusions and superficial micro holes. The fatigue strength curve, solid line in the figures, divides the safe region from the failure region, that is, for loads that generate stresses below this curve, failure is not expected, and failure is expected for stresses above it. Dashed lines represent error bands. Full symbols represent specimens that failed, while empty symbols represent run-outs. Some symbols overlap, indicating stress levels where both, failures and run-outs occurred. Fig. 31 specifically depicts data from 4140 specimens with a microhole, with Fig. 31(a) showing uniaxial and in-phase combined loading conditions with MRH calculated data, Fig. 31(b) depicts uniaxial and in-phase combined loading conditions with MVM calculated data, and Fig. 31 (c) presenting 45° out-of-phase loading conditions.

The comparison shows a conservative trend in all cases. When we look at Fig. 31(a) and 31(b) it becomes clear that when the data is calculated with the MVM, the data is closer to the prediction line, reducing the error, as observed in previous studies. For the data calculated with the MRH, the prediction line begins to correctly divide the safe region from the failure region only with a bandwidth of 30%, while for the data with the MVM, for a bandwidth of 10% or less, the prediction becomes accurate. The exception is the tension-compression data ($\tau_{xya}/\sigma_{xa} = 0$), which does not change with the different methods used to calculate the amplitude of the principal stresses and continues to have a high error in both cases.

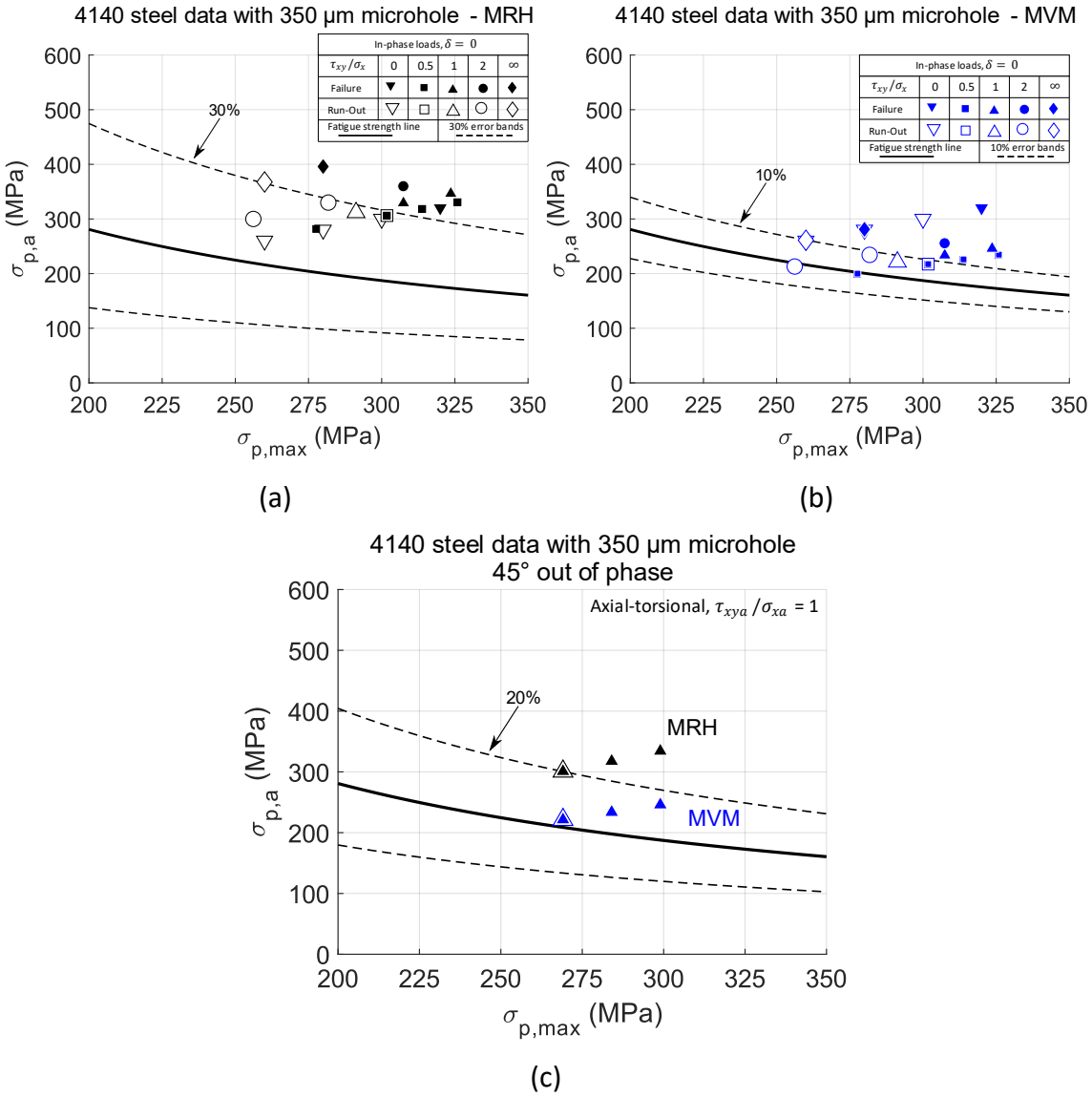

Figure 31. SWT_{mod} prediction and 4140 steel data with 350 µm microhole, (a) uniaxial and in-phase combined data calculated with MRH, (b) uniaxial and in-phase combined data calculated with MVM, and (c) 45° out-of-phase combined loading data.

The comparison of the fatigue data of 4340 steel with the prediction of the new multiaxial model is shown in Fig. 32, where the uniaxial and combined data calculated with the MRH are shown in Fig. 32(a) and the uniaxial and combined data calculated with the MVM are shown in Fig. 32(b).

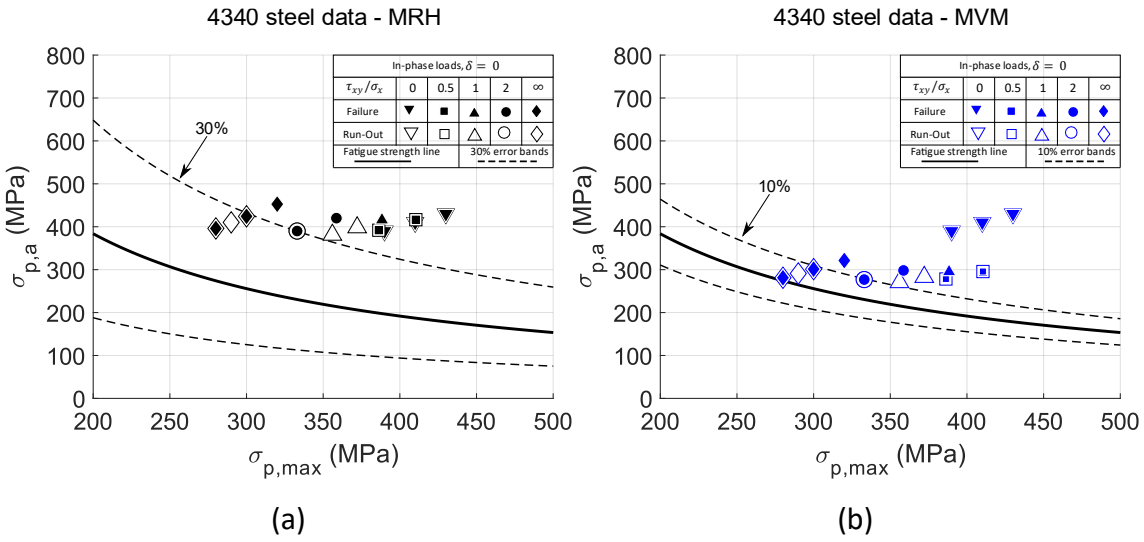

Figure 32. SWT_{mod} prediction and 4340 steel data, (a) uniaxial and in-phase combined data calculated with MRH, and (b) uniaxial and in-phase combined data calculated with MVM.

The same comments made for the 4140 steel data, Fig. 31, are valid for the 4340 steel data, Fig. 32. For the data calculated with the MRH, Fig. 32(a), the prediction line begins to correctly divide the safe region from the failure region only above a bandwidth of 30%, while for the data with the MVM, Fig. 32(b), the required bandwidth to obtain a more accurate division is close to 10%. Also, the exception is the tension-compression data ($\tau_{xya}/\sigma_{xa} = 0$), which does not change with the different methods used to calculate the amplitude of the principal stresses. But it's worth mentioning again that the errors have a conservative tendency, i.e. they favor safety.

5.4.3 Error Index

The accuracy of the criterion is evaluated through the error index, EI, which quantifies the relative difference between the experimental result (R_E) and the predicted result (R_P).

$$EI = \frac{R_E - R_P}{R_P} \times 100\% \tag{33}$$

Although the presentation of results focused primarily on the MRH and MVM methods, other mathematical approaches were also investigated for calculating the

amplitude of the principal stress vector, with the objective of identifying the most accurate and consistent approach for the experimental dataset analyzed. Table 18 presents the mean prediction errors obtained with Eq. 33 when the SWT_{mod} was combined with each method. In addition to the MRH and MVM approaches, the amplitude of the principal stresses was also computed using the Moment of Inertia (MOI) and the Minimum Circumscribed Circumference (MCC) methods, both of which provide distinct formulations to characterize the amplitude.

Table 18. Mean prediction errors of the SWT_{mod} using different methods for principal stress amplitude calculation.

		Mean EI %			
	Loadings	**MRH**	**MVM**	**MOI**	**MCC**
4140 Specimen with a 350 µm microhole	Uniaxial and combined in-phase	23.24	11.10	14.35	17.67
	Combined out-of-phase	20.05	2.97	6.19	13.54
4340 Smooth specimen	Uniaxial and combined in-phase	36.55	21.50	25.49	28.28
All loads		26.61	11.86	15.34	19.83

The proposed model provided conservative predictions when compared to the experimental data across all different calculations. When calculating the amplitude of the principal stresses with the MVM, smaller errors were obtained, with a mean error in general of 11.86%, which is a satisfactory result when it comes to fatigue.

This degree of conservatism may be slightly influenced by the stopping criterion established for the tests. Especially for the tension-compression data, where the greatest errors were obtained, due to the large dispersion of the results, it was not possible to determine the threshold of fatigue resistance experimentally, a much larger number and longer tests would be necessary. Originally, the $\sqrt{area}$ parameter model considers 10^7 cycles as the fatigue limit. However, in this work, the stopping criterion for fatigue tests was defined as 2.10^6, due to operational limitations and reduction in test time.

5.5 Conclusions

Satisfactory results were achieved in the evaluation of the SWT_{mod} with new experimental data from 4140 and 4340 steels. By using the Maximum Variance Method (MVM) to compute the principal stress amplitude, better results were achieved when

compared to the other methods. The average error of the SWT_{mod} by using the MVM for all tests conducted was 11.86%. Notably, all errors observed were conservative, meaning they were in favor of safety.

The SWT_{mod} is capable of predicting fatigue endurance with a focus on a simple, quick, and cost-effective calibration process based on the $\sqrt{area}$ parameter, from which the fatigue limit, σ_w, is derived. Additionally, the calibration of the SWT_{mod} using fatigue limits obtained through the √area parameter allows for the consideration of the influence of small defects on fatigue resistance, without the need to perform tests for each different type of defect.

In conclusion, the new model, coupled with the use of the $\sqrt{area}$ parameter and the MVM, offers a robust approach to fatigue endurance prediction, especially in the presence of small defects. By eliminating the need for exhaustive defect-specific testing, it presents a highly efficient solution for industrial applications, ensuring both accuracy and safety in fatigue design. Further research may investigate the extension of the model to other materials and defect geometries to explore its full potential in multiaxial fatigue loading scenarios.

6. GENERAL CONCLUSIONS AND FUTURE WORK

6.1 Summary of the Main Contributions

The primary objective of this thesis was the development and evaluation of methodologies for estimating the fatigue strength of high-strength steels containing small defects, such as non-metallic inclusions or minor surface discontinuities, with particular focus on proportional and non-proportional multiaxial loading conditions. To this end, two distinct models were assessed: a critical plane criterion previously proposed by Castro et al., and a new multiaxial fatigue model developed as part of this work. Both models were adapted to account for the effects of small defects through calibration using fatigue limits estimated with the $\sqrt{area}$ parameter.

One of the main advances provided by this approach was the demonstration that the fatigue limit used in the newly proposed model, SWT_{mod}, can be the one estimated using the √area parameter. For materials without significant defects, the use of the experimental fatigue limit remains an effective alternative. However, for materials containing small defects, such as the natural non-metallic inclusions found in AISI 4140 and AISI 4340 steels, the use of the fatigue limit derived from the $\sqrt{area}$ parameter is substantially more advantageous, as it not only drastically reduces the costs associated with lengthy testing campaigns but also provides conservative and accurate estimates. This is particularly relevant considering that, in many cases, fatigue limits obtained experimentally may underestimate the influence of small defects due to the high scatter of results, the limited number of test specimens, and the high cost of conducting multiple long-duration fatigue tests.

Another important contribution of this thesis lies in the incorporation of the amplitude of the principal stresses as a key variable in the proposed multiaxial fatigue model. The proposed methodology employs mathematical methods, such as the Maximum Variance Method (MVM), to compute the principal stress amplitude, providing a more physically meaningful representation of the conditions leading to crack initiation in materials with microdefects. This refinement enhances the model's ability to capture the true driving force of fatigue damage in steels containing non-metallic inclusions or surface defects. The adoption of principal stress amplitude represents a novel and relevant advancement in multiaxial fatigue modelling, aligning with

experimental observations that fatigue cracks tend to nucleate on or near planes of maximum principal stress. This approach not only improves prediction accuracy but also contributes to a deeper understanding of fatigue mechanisms in defect-sensitive materials.

Based on the results obtained throughout the articles, the following general conclusions can be highlighted:

- Experimental tests on smooth specimens and specimens with superficial microholes confirmed that, in materials with small defects, fatigue cracks tend to nucleate on planes associated with the maximum normal stress and/or principal stress. This behavior reinforces the appropriateness of using criteria that incorporate principal stress analysis.
- The critical plane model adapted with the $\sqrt{area}$ parameter showed satisfactory performance in predicting fatigue limits and crack initiation directions under different loading conditions. The statistical approach using extreme value theory proved to be effective for estimating the largest defect in samples with natural inclusions, while the direct calculation of $\sqrt{area}$ was sufficient for specimens with surface microholes.
- The proposed multiaxial model (SWT_{mod}) demonstrated great potential for practical applications due to its simple calibration procedure, which requires neither material constants nor S-N curves. It relies only on material hardness and defect geometry. The new model, now incorporating the amplitude of the principal stress via the Maximum Variance Method (MVM), achieved a better representation of the physical phenomenon of crack nucleation in materials with microdefects.
- The validation of the SWT_{mod} model using experimental data for AISI 4140 and AISI 4340 steels under different multiaxial loading conditions showed average errors below 10%, considering the totality of the experimental data, with all predictions being conservative. This result demonstrates the robustness of the model for industrial applications, where safety and speed of estimation are essential.
- The ability to apply the fatigue limit estimated directly from hardness measurements and inclusion characterization via microscopic analysis eliminates the need for exhaustive testing, making the model a promising tool for fatigue

design in real-world components, such as crankshafts for thermoelectric power plants, where internal defects are inevitable.

In summary, the models analyzed and developed in this thesis significantly contribute to the advancement of fatigue design methodologies for defective materials, especially under complex loading conditions. The integration of solid theoretical foundations, comprehensive experimental validation, and practical applicability makes these tools highly relevant to modern engineering design of critical components.

6.2 Suggestions for future work

Based on the results obtained in this thesis, several promising directions for future research can be identified to broaden the scope and applicability of the developed methodologies:

- Study of model sensitivity to defect geometry and orientation:

Test the proposed model with different defect geometries, but maintaining the same $\sqrt{area}$ value. The orientation of defects may influence the accuracy of $\sqrt{area}$-based fatigue limit estimations. Additional studies on the effects of defect morphology and alignment relative to principal stress directions could further refine the model's reliability. Furthermore, evaluating the model against different defect types (e.g., pores, short cracks, elongated holes) would further extend its applicability.

- Extension of the SWT_{mod} model to finite-life fatigue regimes:

Although the proposed model has proven effective in predicting fatigue strength, its application to finite-life conditions has not yet been explored. Future studies could incorporate S-N curves calibrated for different $\sqrt{area}$ or integrate the model with cumulative damage laws, enabling its use for life prediction on components subjected to variable amplitude loading.

- Application to other materials and defect classes:

The investigations in this thesis focused on high-strength steels (AISI 4140 and AISI 4340). Applying the SWT_{mod} model to other materials, such as aluminum alloys,

titanium, or additively manufactured metals, it's a natural path to validate its robustness and generality.

- Evaluation under non-stationary or aleatory multiaxial loading:

A limitation of the current work was the focus on harmonic and stationary multiaxial loadings. Applying the proposed model to aleatory or real-world loading conditions, such as those encountered in automotive crankshafts or turbine blades, would represent a significant advance in practical fatigue design.

- Integration with automated microstructural characterization techniques:

The estimation of the $\sqrt{area}$ parameter could be enhanced using image processing tools and artificial intelligence applied to scanning electron microscopy. This would enable automated and statistically robust identification of the largest internal defects in real components, improving the efficiency and accuracy of model calibration.

7. BIBLIOGRAPHIC REFERENCES

[1] Murakami Y, Endo M. Effects of defects, inclusions and inhomogeneities on fatigue strength. Int J Fatigue 1994;16:163–82. https://doi.org/10.1016/0142-1123(94)90001-9.

[2] Murakami Y. Metal fatigue: Effects of small defects and nonmetallic inclusions. 2019. https://doi.org/10.1016/C2016-0-05272-5.

[3] Nadot Y. Fatigue from Defect: Influence of Size, Type, Position, Morphology and Loading. Int J Fatigue 2022;154. https://doi.org/10.1016/j.ijfatigue.2021.106531.

[4] Zerbst U, Madia M, Klinger C, Bettge D, Murakami Y. Defects as a root cause of fatigue failure of metallic components. I: Basic aspects. Eng Fail Anal 2019;97. https://doi.org/10.1016/j.engfailanal.2019.01.055.

[5] Zerbst U, Madia M, Klinger C, Bettge D, Murakami Y. Defects as a root cause of fatigue failure of metallic components. II: Non-metallic inclusions. Eng Fail Anal 2019;98. https://doi.org/10.1016/j.engfailanal.2019.01.054.

[6] Araujo LC, da Costa RA, Araújo JA, de Castro FC. Effect of natural and artificial defects on multiaxial fatigue of 4140 steel. Int J Fatigue 2024;178. https://doi.org/10.1016/j.ijfatigue.2023.108015.

[7] McEvily AJ. Metal Failures: Mechanisms, Analysis, Prevention. Wiley; 2013.

[8] Endo M, Ishimoto I. The fatigue strength of steels containing small holes under out-of-phase combined loading. Int J Fatigue 2006;28:592–7. https://doi.org/10.1016/j.ijfatigue.2005.05.013.

[9] Schönbauer BM, Yanase K, Endo M. The influence of various types of small defects on the fatigue limit of precipitation-hardened 17-4PH stainless steel. Theoretical and Applied Fracture Mechanics 2017;87:35–49. https://doi.org/10.1016/j.tafmec.2016.10.003.

[10] Yamashita Y, Murakami T, Mihara R, Okada M, Murakami Y. Defect analysis and fatigue design basis for Ni-based superalloy 718 manufactured by selective laser melting. Int J Fatigue 2018;117:485–95. https://doi.org/10.1016/j.ijfatigue.2018.08.002.

[11] Machado PVS, Araújo LC, Soares MV, Reis L, Araújo JA. Multiaxial fatigue assessment of steels with non-metallic inclusions by means of adapted critical plane criteria. Theoretical and Applied Fracture Mechanics 2020;108:102585. https://doi.org/10.1016/j.tafmec.2020.102585.

[12] Evans MH. An updated review: white etching cracks (WECs) and axial cracks in wind turbine gearbox bearings. Materials Science and Technology (United Kingdom) 2016;32. https://doi.org/10.1080/02670836.2015.1133022.

[13] Doglione R, Firrao D. Structural collapse calculations of old pipelines. Int J Fatigue 1998;20. https://doi.org/10.1016/S0142-1123(97)00100-X.

[14] Zerbst U, Klinger C. Material defects as cause for the fatigue failure of metallic components. Int J Fatigue 2019;127. https://doi.org/10.1016/j.ijfatigue.2019.06.024.

[15] Fonte M, de Freitas M. Marine main engine crankshaft failure analysis: A case study. Eng Fail Anal 2009;16. https://doi.org/10.1016/j.engfailanal.2008.10.013.

[16] Murakami Y, Endo M. Effects of Hardness and Crack Geometries on ΔKth of Small Cracks Emanating from Small Defects. In: K.J. Miller and E.R. de los Rios (Eds): The Behaviour of Short Fatigue Cracks. Mech Eng Publ 1986;EGF Publ.:275–93.

[17] Endo M. Effects of small defects on the fatigue strength of steel and ductile iron under combined axial/torsional loading. Small Fatigue Cracks, 1999, p. 375–87. https://doi.org/10.1016/b978-008043011-9/50035-1.

[18] Endo M, Yanase K. Effects of small defects, matrix structures and loading conditions on the fatigue strength of ductile cast irons. Theoretical and Applied Fracture Mechanics 2014;69:34–43. https://doi.org/10.1016/j.tafmec.2013.12.005.

[19] Yanase K, Endo M. Multiaxial high cycle fatigue threshold with small defects and cracks. Eng Fract Mech 2014;123:182–96. https://doi.org/10.1016/j.engfracmech.2014.03.017.

[20] ENDO M, ISHIMOTO I. Effects of Phase Difference and Mean Stress on the Fatigue Strength of Small-Hole-Containing Specimens Subjected to Combined Load. Journal of Solid Mechanics and Materials Engineering 2007;1:343–54. https://doi.org/10.1299/jmmp.1.343.

[21] Nadot Y, Billaudeau T. Multiaxial fatigue limit criterion for defective materials. Eng Fract Mech 2006;73:112–33. https://doi.org/10.1016/j.engfracmech.2005.06.005.

[22] Billaudeau T, Nadot Y, Bezine G. Multiaxial fatigue limit for defective materials: Mechanisms and experiments. Acta Mater 2004;52:3911–20. https://doi.org/10.1016/j.actamat.2004.05.006.

[23] Nasr A, Nadot Y, Bouraoui C, Fathallah R. Fatigue life assessment for material containing defects under multiaxial loading. Metallurgical Research and Technology 2017;114. https://doi.org/10.1051/metal/2016060.

[24] Sanaei N, Fatemi A. Defects in additive manufactured metals and their effect on fatigue performance: A state-of-the-art review. Prog Mater Sci 2021;117. https://doi.org/10.1016/j.pmatsci.2020.100724.

[25] Foti P, Mohammad Javad Razavi S, Fatemi A, Berto F. Multiaxial fatigue of additively manufactured metallic components: A review of the failure mechanisms and fatigue life prediction methodologies. Prog Mater Sci 2023;137. https://doi.org/10.1016/j.pmatsci.2023.101126.

[26] Wang J, Zhang M, Wang B, Tan X, Wu WJ, Liu Y, et al. Influence of surface porosity on fatigue life of additively manufactured ASTM A131 EH36 steel. Int J Fatigue 2021;142. https://doi.org/10.1016/j.ijfatigue.2020.105894.

[27] Wang Y, Su Z. Effect of micro-defects on fatigue lifetime of additive manufactured 316L stainless steel under multiaxial loading. Theoretical and Applied Fracture Mechanics 2021;111. https://doi.org/10.1016/j.tafmec.2020.102849.

[28] Araújo LC, Machado PVS, Pereira MVS, Araújo JA. An alternative approach to calibrate multiaxial fatigue models of steels with small defects. Procedia Structural Integrity, vol. 19, 2019, p. 19–26. https://doi.org/10.1016/j.prostr.2019.12.004.

[29] Araujo LC, de Oliveira D, Pereira MVS, Araújo JA. Adapted multiaxial fatigue models based on the critical plane approach to consider the presence of small defects in steel. Procedia Structural Integrity 2022;42. https://doi.org/10.1016/j.prostr.2022.12.020.

[30] Vantadori S, Ronchei C, Scorza D, Zanichelli A, Araújo LC, Araújo JA. Influence of non-metallic inclusions on the high cycle fatigue strength of steels. Int J Fatigue 2022;154. https://doi.org/10.1016/j.ijfatigue.2021.106553.

[31] Scorza D, Carpinteri A, Ronchei C, Vantadori S, Zanichelli A. Effect of non-metallic inclusions on AISI 4140 fatigue strength. Int J Fatigue 2022;163. https://doi.org/10.1016/j.ijfatigue.2022.107031.

[32] Araujo LC, Oliveira D de, Araújo JA. A New Multiaxial Fatigue Model for High Strength Steels Taking into Account the Presence of Small Defects. Proceedings of the13th International Conference on Multiaxial Fatigue and Fracture (ICMFF13), 2022.

[33] Castro FC, Mamiya EN, Bemfica C. A critical plane criterion to multiaxial fatigue of metals containing small defects. Journal of the Brazilian Society of Mechanical Sciences and Engineering 2021;43. https://doi.org/10.1007/s40430-021-03246-4.

[34] Dias AL, Bemfica C, Castro FC. Multiaxial high cycle fatigue of 304L stainless steel with a small defect. Int J Fatigue 2022;156. https://doi.org/10.1016/j.ijfatigue.2021.106698.

[35] Araujo LC, Malcher L, de Oliveira D, Araújo JA. A new multiaxial fatigue endurance model for high strength steels taking into account the presence of small defects. Int J Fatigue 2024;178. https://doi.org/10.1016/j.ijfatigue.2023.107981.

[36] Araujo LC, Ferreira JL de A, Ziberov M, Araújo JA. Assessing Fatigue in Materials with Small Defects: A New Multiaxial Model Based on Principal Stress Amplitudes. Procedia Structural Integrity 2024;57:144–51. https://doi.org/10.1016/j.prostr.2024.03.017.

[37] Murakami Y. Inclusion rating by statistics of extreme values and its application to fatigue strength prediction and quality control of materials. J Res Natl Inst Stand Technol 1994;99:345. https://doi.org/10.6028/jres.099.032.

[38] Vantadori S, Ronchei C, Scorza D, Zanichelli A, Luciano R. Effect of the porosity on the fatigue strength of metals. Fatigue Fract Eng Mater Struct 2022;45. https://doi.org/10.1111/ffe.13783.

[39] Endo M, McEvily AJ. Fatigue crack growth from small defects under out-of-phase combined loading. Eng Fract Mech 2011;78:1529–41. https://doi.org/10.1016/j.engfracmech.2010.12.011.

[40] Beretta S, Murakami Y. Statistical analysis of defects for fatigue strength prediction and quality control of materials. Fatigue Fract Eng Mater Struct 1998;21:1049–65. https://doi.org/10.1046/j.1460-2695.1998.00104.x.

[41] Beretta S. More than 25 years of extreme value statistics for defects: Fundamentals, historical developments, recent applications. Int J Fatigue 2021;151. https://doi.org/10.1016/j.ijfatigue.2021.106407.

[42] Beretta S, Murakami Y. SIF and threshold for small cracks at small notches under torsion. Fatigue Fract Eng Mater Struct 2000;23:97–104. https://doi.org/10.1046/j.1460-2695.2000.00260.x.

[43] Dowling NE. Mean stress effects in strain-life fatigue. Fatigue Fract Eng Mater Struct 2009;32. https://doi.org/10.1111/j.1460-2695.2009.01404.x.

[44] Socie DF, Marquis GB. Multiaxial Fatigue. SAE International; 2000.

[45] Socie DF, Hua CT, Worthem DW. MIXED MODE SMALL CRACK GROWTH. Fatigue Fract Eng Mater Struct 1987;10. https://doi.org/10.1111/j.1460-2695.1987.tb01145.x.

[46] Jiang Y, Hertel O, Vormwald M. An experimental evaluation of three critical plane multiaxial fatigue criteria. Int J Fatigue 2007;29. https://doi.org/10.1016/j.ijfatigue.2006.10.028.

[47] Castro F, Jiang Y. Fatigue life and early cracking predictions of extruded AZ31B magnesium alloy using critical plane approaches. Int J Fatigue 2016;88. https://doi.org/10.1016/j.ijfatigue.2016.04.002.

[48] McDowell DL, Dunne FPE. Microstructure-sensitive computational modelling of fatigue crack formation. Int J Fatigue 2010;32. https://doi.org/10.1016/j.ijfatigue.2010.01.003.

[49] Papadopoulos I V. Fatigue polycyclique des métaux: une nouvelle approche. Thèse de Doctorat. Ecole Nationale des Ponts et Chaussées, 1987.

[50] Papadopoulos I V. Critical plane approaches in high-cycle fatigue: On the definition of the amplitude and mean value of the shear stress acting on the critical plane. Fatigue Fract Eng Mater Struct 1998:269–85.

[51] Papuga J. A survey on evaluating the fatigue limit under multiaxial loading. Int J Fatigue 2011;33. https://doi.org/10.1016/j.ijfatigue.2010.08.001.

[52] Papadopoulos I V., Davoli P, Gorla C, Filippini M, Bernasconi A. A comparative study of multiaxial high-cycle fatigue criteria for metals. Int J Fatigue 1997;19. https://doi.org/10.1016/S0142-1123(96)00064-3.

[53] Mamiya EN, Castro FC, Araújo JA. Recent developments on multiaxial fatigue: The contribution of the University of Brasília. Theoretical and Applied Fracture Mechanics 2014:48–59. https://doi.org/10.1016/j.tafmec.2014.06.007.

[54] Murakami Y, Nemat-Nasser S. Growth and stability of interacting surface flaws of arbitrary shape. Eng Fract Mech 1983;17:193–210. https://doi.org/10.1016/0013-7944(83)90027-9.

[55] Murakami Y. Material defects as the basis of fatigue design. Int J Fatigue, vol. 41, 2012, p. 2–10. https://doi.org/10.1016/j.ijfatigue.2011.12.001.

[56] Castro FC, Mamiya EN, Bemfica C. A critical plane model to multiaxial fatigue of metals containing small defects. Brasília - DF: 2019.

[57] Groza M, Nadot Y, Varadi K. Defect size map for nodular cast iron components with ellipsoidal surface defects based on the defect stress gradient approach. Int J Fatigue 2018;112:206–15. https://doi.org/10.1016/j.ijfatigue.2018.03.025.

[58] Karolczuk A, Nadot Y, Dragon A. Non-local stress gradient approach for multiaxial fatigue of defective material. Comput Mater Sci 2008;44:464–75. https://doi.org/10.1016/j.commatsci.2008.04.005.

[59] Ronchei C. Fatigue Strength Estimation of Ductile Cast Irons Containing Solidification Defects. Metals (Basel) 2023;13. https://doi.org/10.3390/met13010083.

[60] Tanaka K, Akiniwa Y. Fatigue crack propagation behaviour derived from S-N data in very high cycle regime. Fatigue Fract Eng Mater Struct 2002;25. https://doi.org/10.1046/j.1460-2695.2002.00547.x.

[61] Shiozawa K, Hasegawa T, Kashiwagi Y, Lu L. Very high cycle fatigue properties of bearing steel under axial loading condition. Int J Fatigue 2009;31. https://doi.org/10.1016/j.ijfatigue.2008.11.001.

[62] Lambrighs K, Verpoest I, Verlinden B, Wevers M. Influence of non-metallic inclusions on the fatigue properties of heavily cold drawn steel wires. Procedia Eng, vol. 2, 2010. https://doi.org/10.1016/j.proeng.2010.03.019.

[63] Shiozawa K, Murai M, Shimatani Y, Yoshimoto T. Transition of fatigue failure mode of Ni-Cr-Mo low-alloy steel in very high cycle regime. Int J Fatigue 2010;32. https://doi.org/10.1016/j.ijfatigue.2009.06.011.

[64] Yakura R, Matsuda M, Sakai T, Ueno A. Effect of inclusion size on fatigue properties in very high cycle region of low alloy steel used for solid-type crankshaft. R and D: Research and Development Kobe Steel Engineering Reports 2016;66.

[65] Murakami Y, Toriyama T, Coudert EM. Instructions for a new method of inclusion rating and correlations with the fatigue limit. J Test Eval 1994;22:318–26. https://doi.org/10.1520/jte11840j.

[66] Yanase K, Endo M. Prediction for multiaxial fatigue strength with small defects. MATEC Web of Conferences, 2014, p. 2. https://doi.org/10.1520/MPC20130013.

[67] Smith KN, Topper TH, Watson P. A stress–strain function for the fatigue of metals. J Materials 1970;5:767–78. https://doi.org/10.1179/1752270612Y.0000000008.

[68] Dowling NE. Mechanical Behavior of Materials - Engineering Methods for Deformation, Fracture, and Fatigue. Fourth Edi. International Edition: Pearson Education Limited; 2013.

[69] Araújo JA, Dantas AP, Castro FC, Mamiya EN, Ferreira JLA. On the characterization of the critical plane with a simple and fast alternative measure of the shear stress amplitude in multiaxial fatigue. Int J Fatigue 2011;33:1092–100. https://doi.org/10.1016/j.ijfatigue.2011.01.002.

[70] Bolar G, Adhikari R, Nayak SN, Joshi SN. Assessment of ignition risk in dry helical hole milling of AZ31 magnesium alloy considering the machining temperature and chip morphology. J Manuf Process 2022;77. https://doi.org/10.1016/j.jmapro.2022.03.023.

[71] Nickel J, Baak N, Biermann D, Walther F. Influence of the deep hole drilling process and sulphur content on the fatigue strength of AISI 4140 steel components. Procedia CIRP, vol. 71, 2018. https://doi.org/10.1016/j.procir.2018.05.069.

[72] Abouridouane M, Klocke F, Lung D, Adams O. Size effects in micro drilling ferritic-pearlitic carbon steels. Procedia CIRP, vol. 3, 2012. https://doi.org/10.1016/j.procir.2012.07.017.

[73] de Oliveira D, Gomes MC, da Silva MB. Influence of cutting fluid application frequency on the surface quality of micromilled slots on Inconel 718 alloy. vol. 48, 2020. https://doi.org/10.1016/j.promfg.2020.05.082.

[74] Arrabiyeh PA, Heintz M, Kieren-Ehses S, Bohley M, Kirsch B, Aurich JC. Submerged micro grinding: a metalworking fluid application study. International Journal of Advanced Manufacturing Technology 2020;107. https://doi.org/10.1007/s00170-020-05240-x.

[75] Ferreira JLA, Dias JN, Cardoso EU, Araújo JA, da Silva CRM. A contribution to the identification of the critical plane using the maximum variance method. Int J Fatigue 2022;165. https://doi.org/10.1016/j.ijfatigue.2022.107228.

[76] Dang Van K, Griveau B, Message O. On a new multiaxial fatigue limit criterion: Theory and application. In: Brown MW, Miller KJ, editors. Biaxial and Multiaxial Fatigue, EGF 3, London: Mechanical Engineering Publications; 1989, p. 479–96.

[77] Li B, Santos JLT, De Freitas M. Unified numerical approach for multiaxial fatigue limit evaluation. Mechanics of Structures and Machines 2000;28:85–103. https://doi.org/10.1081/SME-100100613.

[78] Meggiolaro MA, Castro JTP De. The moment of inertia method to calculate equivalent ranges in non-proportional tension – torsion histories. Integr Med Res 2015;4:229–34. https://doi.org/10.1016/j.jmrt.2015.01.004.

[79] Wu H, Meggiolaro MA, Castro JTP De. Application of the Moment Of Inertia method to the Critical-Plane Approach. Frattura Ed Integrità Strutturale 2016;38:99–105. https://doi.org/10.3221/IGF-ESIS.38.13.

[80] Mamiya EN, Araújo JA, Castro FC. Prismatic hull: A new measure of shear stress amplitude in multiaxial high cycle fatigue. Int J Fatigue 2009;31:1144–53. https://doi.org/10.1016/j.ijfatigue.2008.12.010.

[81] Stephens RI, Fatemi A, Stephens RR, Fuchs HO. Metal Fatigue in Engineering. 2nd ed. 2001. https://doi.org/10.1016/j.jpolmod.2011.03.005.

[82] Grubisic V, Simbürger A. Fatigue under combined out of phase multiaxial stresses. International Conference on Fatigue Testing and Design, London: 1976, p. 27.1-27.8.